

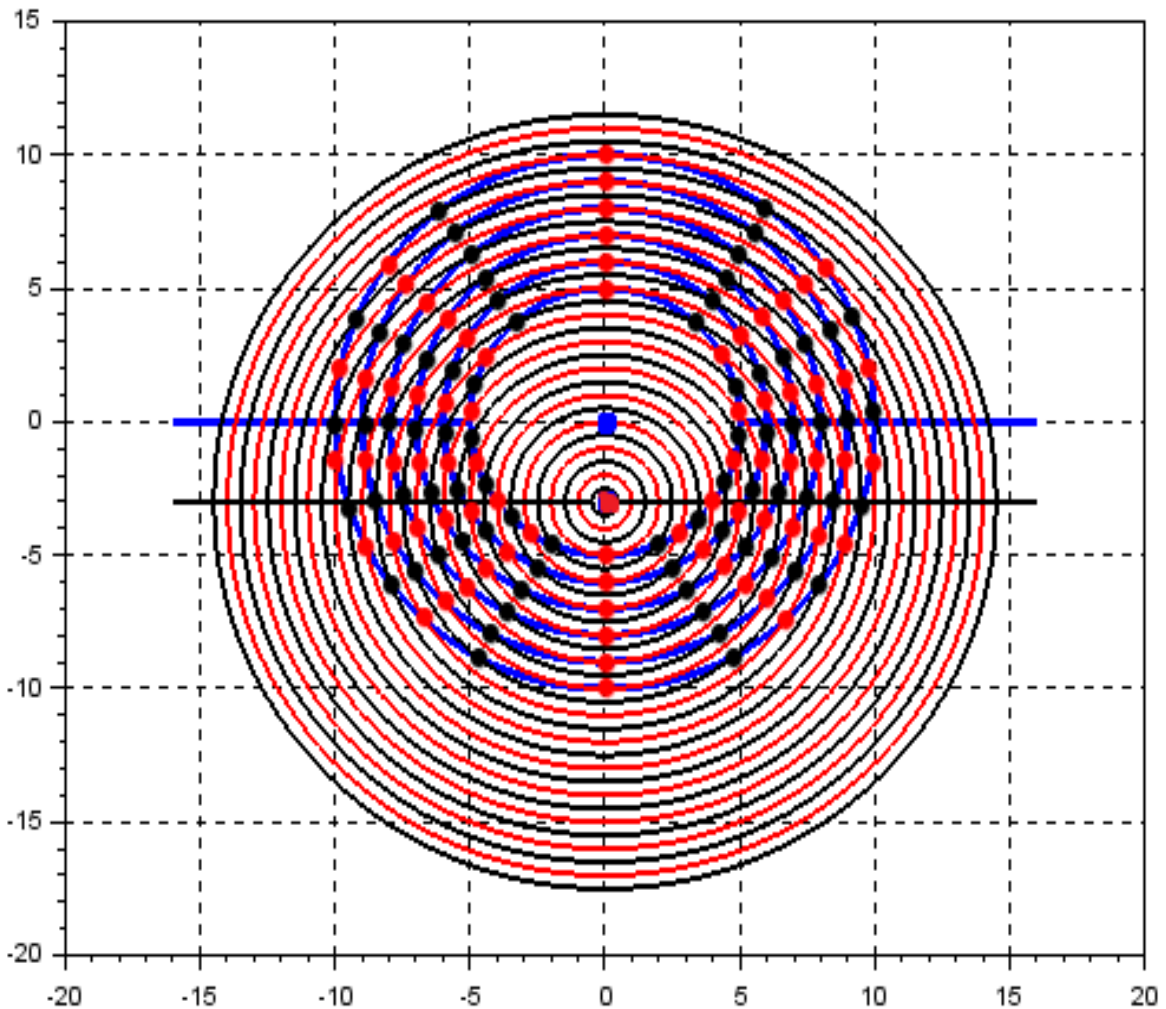
**ISSN 0970-5953**



**Volume 35. No. 2**

**April - June 2019**

# PHYSICS EDUCATION



***www.physedu.in***

---

**Volume 35, Number 2****In this Issue**

- **Editorial** 01 Page  
  
M. S. Santhanam
  
- **A Pedagogical Experiment on Longitudinal Modes of a He-Ne Laser** 07 Pages  
  
S. Ganci, D. Lagomarsino Oneto
  
- **Simulating the Phenomenon of Interference using SCILAB** 10 Pages  
  
Pragati Ashdhir, Neha Batra, Nishant Goyal, Mritunjay Tyagi
  
- **Young's Modulus using Wind Chimes** 07 Pages  
  
Shirish Pathare, Sharvani Shahapurkar
  
- **Market analysis using three state Ising model** 08 Pages  
  
Lisha Damodaran , K. M. Udayanandan
  
- **Exploring the non-linear Oscillations by means of the Law of Energy Conservation: two examples** 06 Pages  
  
V. Ivchenko
  
- **Generalized Lissajous Figures** 07 Pages  
  
Rakesh Kumar Pandey

## EDITORIAL

---

---

The Draft of New Education Policy was submitted to the government by the end of May 2019. Quite expectedly, it has kicked off a bigger debate on various issues related to primary, middle and higher education levels.

As far as higher education and research is concerned, the policy document makes new recommendations. For instance, it proposes that higher education institutions can be permitted through a new body called the National Higher Education Regulation Authority. It also recommends that all new institutions permitted by this authority must be accredited by NAAC within five years. In the core area of education, the policy also makes a strong case for liberal education, which will have a judicious combination of core areas and one or two specialization. There is also a dire need to increase the quantum of funding for education. The draft policy seeks to double the investment in education.

In order to streamline research funding, the policy document recommends establishing a

National Research Foundation “for funding, mentoring and building the capacity for quality research in India”. It is hoped that this prescription would enhance the research base in the country.

The draft policy is certain to be debated and discussed in the coming months. As the debate progresses and as we see how the policy translates in to practice, we will have an opportunity to revisit the salient action points of the draft policy. In particular, its effect on science education both at the school and college level is of particular interest to us. As this moves on, we will also publish expert opinions on our webspecials.

M. S. Santhanam  
Chief Editor  
*Physics Education*

# A Pedagogical Experiment on Longitudinal Modes of a He-Ne Laser

S. Ganci and D. Lagomarsino Oneto

Studio di Catalogazione e Conservazione Strumenti Scientifici

Via “Grazia Deledda 19, A-2

27029 Tromello –PV, Italy

museodellascienza.s.ganci@gmail.com

*Submitted on 08-07-2018*

## Abstract

A He-Ne laser has several longitudinal modes in the stationary waves establishing between the two mirrors constituting its optical cavity. These different wavelengths are inside the ‘natural’ width of the red spectroscopic line of Ne. This paper discusses three different experiments (suitable as demonstration experiments) in order to give simple analysis of the photocurrent revealed by a fast photodiode.

acronym loser were would be equivalent, because a stationary 'wave of light' (having nodes of electric field  $E$  at the mirror surfaces) is establishing in an optical cavity. As elementary condition of a stationary wave in everywhere closed cavity, the condition of an integer number of half wavelengths having nodes at the extreme of the cavity must be satisfied. So, if a cavity has length  $L$ , (distance between the two parallel mirrors) the condition:

$$m \frac{\lambda}{2} = L \quad \text{or} \quad f = \frac{mc}{2L} \quad (1)$$

must be fulfilled and where  $m$  is an integer,  $\lambda$  is the wavelength,  $L$  is the length of the resonant cavity,  $c$  is the speed of the light in empty space and  $f$  its frequency. For an optical cavity (the two laser's mirrors giving a Fabry-Perot cavity).

## 1. Introduction

The diffusion of low-cost and low-power He-Ne laser in high school laboratory as a versatile light source with high spatial and temporal coherence makes necessary an intuitive and elementary treatment of the stimulated emission process as elementarily described in the J. R. Meyer-Arendt textbook [1]. It should be pedagogically useful to observe that in acronym of the word laser (Light Amplification by Stimulated Emission of Radiation) emphasis is put on the amplification process by stimulated emission that happens to Neon atoms in a metastable state [1]. However, the

## 2. Elementary theory of the light's stationary wave in a cavity.

Eq. (1) holds approximately because refraction index of He-Ne mixture is assumed constant in time and unity. One of the two laser's plane mirror has a limited reflectivity because it must permit the exit of the light beam. Therefore it is possible to coexist

beyond the condition Eq. (1) also very slightly shorter and upper wavelengths  $\pm\lambda_1\pm\lambda_2\dots$  still fulfilling Eq. (1). These wavelengths represent the longitudinal modes of the electric field  $E$  into the cavity up to the oscillation threshold condition [2] into the intensity function representing the width of the spontaneous Ne 'red' emission. Fabry-Perot cavity of the laser discriminates different wavelengths existing inside the 'natural' width of the spectroscopic red line of excited Ne. Therefore, these wavelengths can superposing pair by pair between them [2, 3] giving a superposition modulated like a beat. Because the beat is a wave of the same spectrum of the two superposing waves it is possible that the superposition can be out the width of the optical radiation and enters the domain of 'radio' waves. An acoustical analogy can be pedagogically useful. Two ultrasounds 40 kHz and 41 kHz emitted from two excited ordinary transducers are singly not heard by the student but its superposition give a (faint but well perceptible) 1 kHz whistle. Ears do not perceive each acoustical perturbation but the superposed signal enters the width of human hearing perception. So, the electric fields  $E_1(t)$  and  $E_2(t)$  of each single light wavefield is undetected by a fast photodiode [4] even its superposition  $E(t) = E_1(t) + E_2(t)$  enters the domain of frequencies perceived by the photodiode itself.

Elementary theory can be developed as below: let us consider two stationary waves of frequencies  $f_1$  and  $f_2$  into the optical cavity and having two nodes of the electric field at the two mirrors. The beat frequency  $f_B$  that our photodiode is engaged to detect is:

$$f_B = |f_1 - f_2| \quad (2)$$

That, for ordinary low power laser used in Lab's School enters the domain of UHF 'radio' waves.

### 3. The various feasible experimental solutions in a high school Lab.

There are almost four experimental simple setups for showing (and measuring) the beats between longitudinal modes:

- a) Using an oscilloscope and a high-frequency generator tuned as a local oscillator mixing it with signal coming from a fast photodiode detector; [5]
- b) Using an old analogic TV; [8, 9]
- c) Using a H. F. spectrum analyzer; [10, 12]
- d) Using a DVB-TDAB+FM+SDR USB dongle with HDSDR spectrum analyzer software working under Windows 7 or Windows 8 or 8.1. At the present, we do not found drivers/software working under Windows 10. [11-12].

b) Because the method a) appears pedagogically hard in a high school, the simplest experimental setup uses a photometric circuit (Fig. 1 a) Photometric detector circuit is shown in Fig. 1 b). The output of the photometric circuit is directly connected to the antenna socket of an old analogic TV. The laser beam is centered with care on the fast photodiode. The signal from the reverse-biased photodiode is applied to the TV antenna through a little value capacitor cutting continuous components into the socket antenna of a little analogic bw TV [6, 7]. Silicon fast photodiodes Hamamatsu S5972-01 and Hamamatsu S9073-02 are low-cost and well suited to the experiment. If the analogic tuning scans the entire UHF width and meantime the fingers runs periodically through the LASER beam, it happens a suddenly modulation of the light (and in the audio noise) in the screen similar to that shown in Fig. 2. Because it happens on a well-defined frequency, we can know

approximately the transmitting channel and therefore the frequency of the beat.

c) If your School Lab has a high frequency spectrum analyzer the measurement of the beat frequency is more simplified. We tried an old spectrum analyzer (Unahom EP738A) with a frequency width from 47 MHz to 800 MHz. The photometric circuit in Fig. 1 b) is connected to the BNC input and the search of tune is very simple. A well-defined peak as shown in Fig. 3 gives, for our laser (LSW 10), a beat frequency  $f_B = 610$  MHz with an uncertainty of about  $\pm 10$  MHz estimated in the peak's width around its base.

d) Finally, we repeat the experiment using a Terratek DVB-TDAB+FM+SDR USB 2.0 dongle with HSDR spectrum analyzer software well working under Windows 7 / Windows 8 or 8.1 [10]. This device is very inexpensive, it needs the driver "Zadig" [11] and HSDR software is easily downloadable from [13]. A screenshot of the beat signal is shown in Fig. 4. It shows in the upper "waterfall" width a little aleatory sliding in time of the beat frequency and a definite peak in the lower width, where the frequency scale is drawn. The trace slow slides in time and, sometimes, jumps as shown in waterfall width; so still give an uncertainty of the frequency around  $\pm 10$  MHz in spite the frequency scale has a so high resolution. As shown in the Literature quoted [8, 9] the analysis of laser modes is not at all so simple as our experiments seems suggest.

#### 4. Conclusions.

The first (b) and the second experiments (c) were almost simple and convincing when used in the classroom as demonstration experiments. Even today, the student is best experienced with the use of PC used as instrument tool through a suitable

software, the use of HSDR device has *vice-versa* induced a bit of confusion and questions of not easy treatment out the context of a simple pedagogic lesson. Probably this third experiment and /or the analysis of the photocurrent, particularly for longer cavity lasers, is out a simple treatment and would be more suitable in an undergraduate course of Optoelectronics.

#### Acknowledgements.

Sincere thanks to Mrs. Karen Rossi for her valuable revision of English language. Thanks to Mr. Marco Bacigalupo for supplying us his personal Unahom spectrum analyzer.

#### References:

- [1]. J. R. Meyer-Arendt, *Introduction to Classical and Modern Optics*, (Prentice-Hall, Englewood Cliffs, N. J. 1972), Chap. 5.5.
- [2] G. R. Fowles, *Introduction to Modern Optics*, 2nd Ed. (Dover, New York, 1975) pp. 274-275.
- [3] N. Kalitévski, *Optique Ondulatoire*, (Mir, Moscow, 1980), chap 5.
- [4] Optical frequencies are of the order of  $10^{14}$  Hz. A 'fast' photodiode is an optoelectronic device that follows the temporal periodic change of the electric field in the superposition of 'two coherent light's wavefronts' whose wavelengths differ about one hundredth of a wavelength between them. So, beat frequency enter the domain of the optoelectronic device.
- [5] D. A. Robinson, "Detector for axial laser modes", *Am. J. Phys.* **43**, 652 (1975).

[6] P. Ottonello and C. Pontiggia, “*Analisi della fotocorrente dovuta a una sorgente laser a gas*”, G. Fis. **14**, 187-191 (1973).

[7] S. Ganci, “Alcune osservazioni sul fenomeno dei battimenti”, G. Fis. **45**, 111-115, (2004).

[8] R. A. Phillips, R. D. Gehrz, “*Laser Mode Structure Experiments for Undergraduate Laboratories*”, Am. J. Phys. **38**, 429-433 (1970)

[9] K. S. Bathia, “*Study of longitudinal mode structure of laser by optical spectrum analyzer*”, Am. J. Phys. **52**, 738-741 (1984).

[10] i.e. available on <http://www.digisat.to.it/> at very low cost.

[11] <https://www.rtl-sdr.com/tag/zadig/>

[12] <http://www.hdsdr.de/>

### Figures and captions.

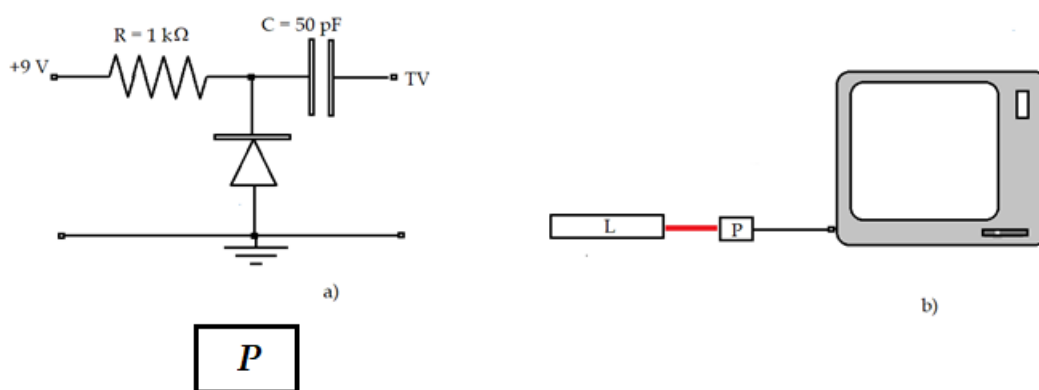


**Fig. 1.** Experimental setup to detect optical beats.

Fig. 1. a) Photometric circuit P. We tried ‘fast’ photodiode Motorola MFOD100, Hamamatsu S5972 and Hamamatsu S9055 Si photodiodes having respectively over 500 MHz and 1.5 GHz for electric field variations in time. In addition, one of the two junctions of a planar epitaxial high frequency transistor, to which the container head has been removed, can work if the school has low budget.

b) Experimental setup. L: He-Ne LASER; P: photometric circuit connected to the socket of TV antenna (syntonizer on VHF for cavity length between 0.22m and 0.3 m).

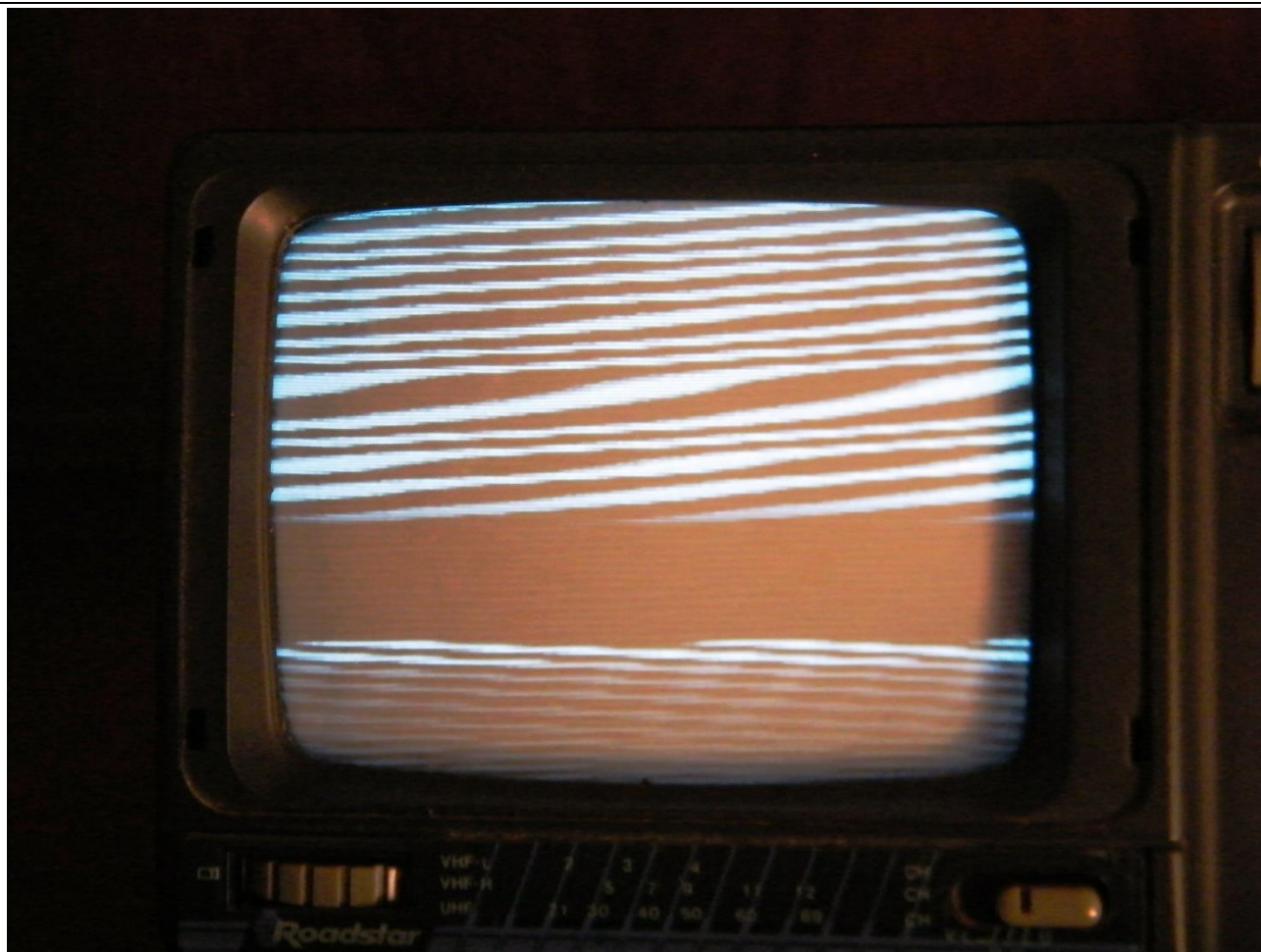


Fig. 2. Typical modulation of the TV screen's light when the tuning is accordingly with beat frequency and the fingers pass periodically through the LASER beam.

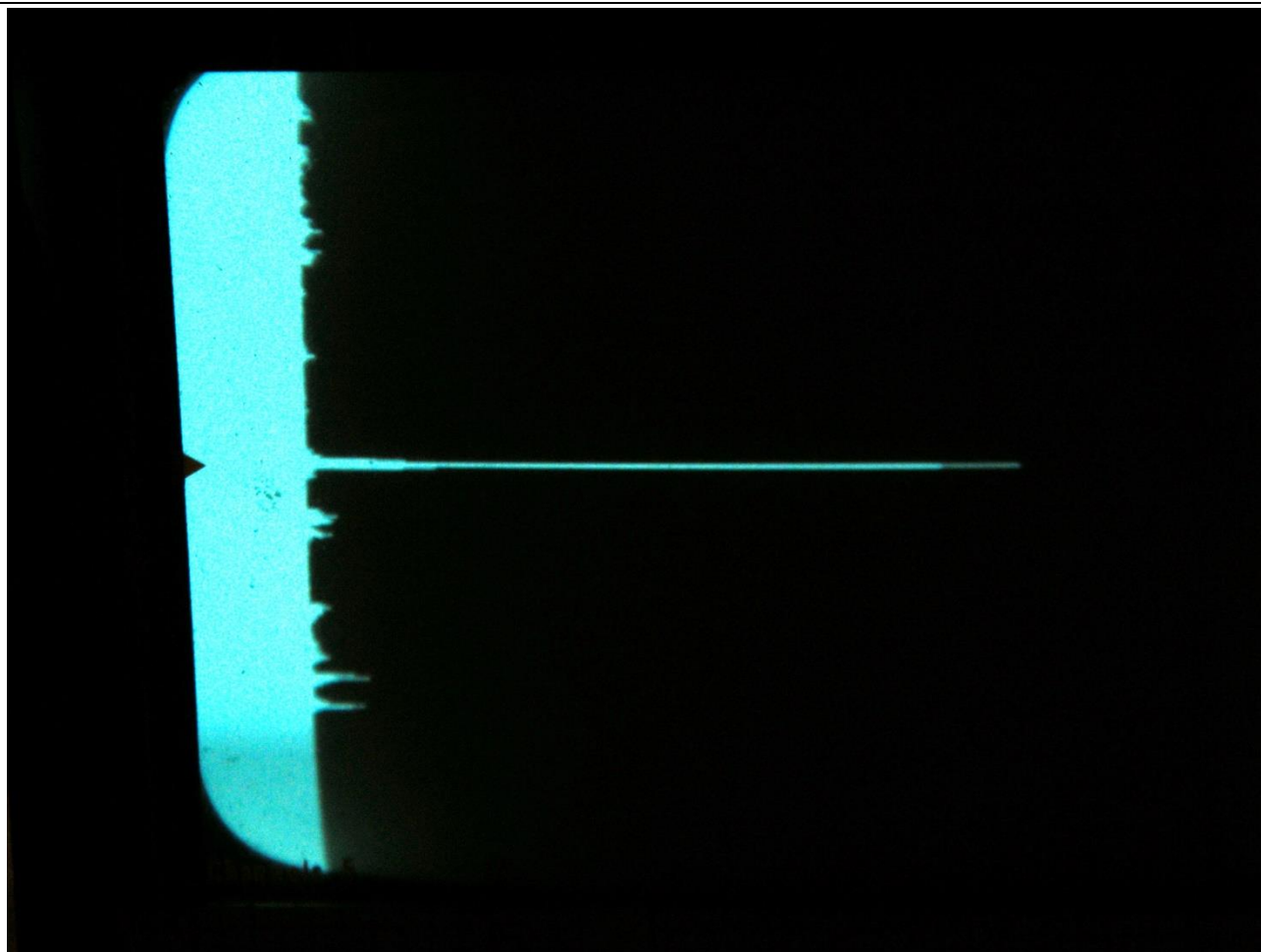


Fig. 3. The peak given by photometric circuit in Fig. 2b when spectrum analyzer is in tune with the beat frequency. For our JXSL Tech. LSW10 He-Ne 1.5 mW, randomly polarized LASER, the beat frequency is estimated in  $610 \text{ MHz} \pm 10 \text{ MHz}$ . The uncertainty is estimated by the width of the peak near its basis.

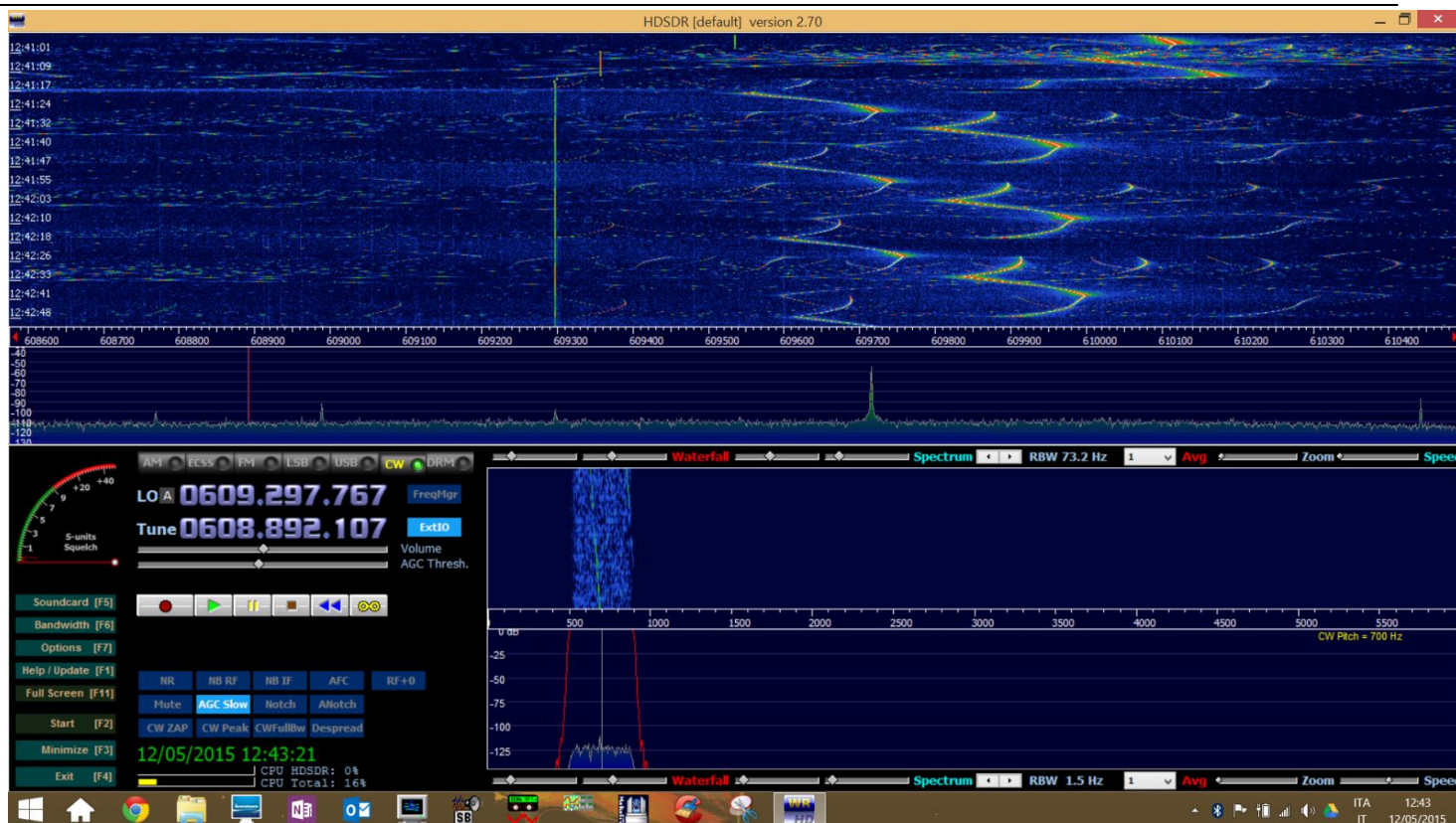


Fig. 4. The peak of the beat caused by two longitudinal modes in our LSW 10 LASER. The “waterfall” window shows as the peak of the frequency (about 609 MHz) aleatory in time changes in time. The main peak in the upper width shows the tune of the beat frequency. It slides, or better *jumps*, among contiguous frequencies in time.

---

# Simulating the Phenomenon of Interference using Scilab

Pragati Ashdhir, Neha Batra, Nishant Goyal, Mritunjay Tyagi

Department of Physics, Hindu College,  
University of Delhi, Delhi-110007

pragatiashdhir@hinducollege.ac.in

*Submitted on 10-12-2018*

## **Abstract**

Introduction of some very fundamental concepts in Physics to students is often a challenge for the teacher, particularly, in situations where direct demonstration or experimentation is not feasible inside the classroom. Interference of waves is one such concept. One of the aims of the proposed work is to show how the concept of interference of waves can be introduced using simulations. The other aim is to illustrate how SCILAB can be used to enable technology based teaching of Physics. In the first part of the work, the phenomenon of interference of waves coming from two point sources is simulated using SCILAB. The later part of the work simulates the interference pattern obtained in Young's Double Slit Experiment using two point sources.

---

## **I. INTRODUCTION**

SCILAB is a free and open-source, numerical computational package, an alternative to MATLAB, which is a proprietary programming language. In the recent syllabi revision of various undergraduate programs offered by some Indian Universities under the Choice Based Credit System (CBCS), programming in SCILAB has been introduced.

The analytical solutions to various problems in physics often have their own limitations and the teacher finds it challenging to explain the practical aspects of these problems to students. Such

situations can however be overcome by using computational physics techniques. SCILAB provides a very powerful and effective platform for the same.

The present work seeks to highlight how SCILAB can be used for a more effective teaching-learning process, through a simple illustration of how the concept of 'Interference of Waves' can be explained rather concretely.

When two sets of waves are made to cross each other, interesting and complicated effects are observed. These effects are explained and understood in terms of the phenomenon of interference which is characteristic of any kind of wave motion. This makes "interference of waves" as one of the fundamental concepts in physics.

The first part of the work illustrates the use of simulations in introducing the concept of interference of waves in classroom at the secondary school or introductory undergraduate level.

The later part of the work simulates the interference pattern obtained in Young's double slit experiment, which is the very first experiment introduced to students on "interference of light". A very in-depth discussion of the interference pattern is done that is often missing in textbooks.

## **II. SUPERPOSITION OF WAVES**

It is a matter of common experience that two trains of ripples on the surface of water cross each other and proceed onward in their directions undisturbed. In the regions of crossing there are places where the disturbance is practically zero and others where it is greater than that given by either wave alone. The

effects are explained by the principle of “superposition of waves”. This principle states that **when a medium is disturbed simultaneously by any number of waves, the instantaneous resultant displacement of the media at every point at every instant is the algebraic sum of the displacement of the medium due to individual waves in the absence of the others.**

Suppose due to a single wave train, the displacement of the medium at a certain point at any instant is  $y_1$  in a given direction and that due to another wave train in the absence of the first, the displacement is  $y_2$ . By the principle of superposition, the instantaneous resultant displacement  $R$  of the medium at that point due to the two waves acting together is

$R=y_1+y_2$ ; if  $y_1$  and  $y_2$  are in the same direction  
 $=y_1-y_2$ ; if  $y_1$  and  $y_2$  are in opposite directions and  $y_1>y_2$   
 $=y_2-y_1$ ; if  $y_1$  and  $y_2$  are in opposite directions and  $y_2>y_1$

This is shown in Figure 1 below.

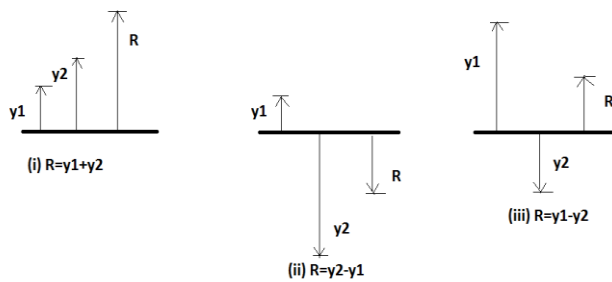


**Figure (1):** Illustration of Principle of Superposition of waves

The validity of this principle is established when it is observed that after the waves have passed out of the region of crossing, they appear to have been entirely uninfluenced by the other set of waves. Amplitude, frequency, and all other characteristics are just as if they had crossed an undisturbed space.

### III. THE INTERFERENCE PHENOMENON

The interference of waves causes the medium to take on a shape that results from the net effect of the two individual waves upon the particles of the medium. At any location along the medium where the two superimposing waves have a path difference equal to an integral multiple of wavelength, constructive interference of waves is said to take place. So,

$$\text{Path difference} = n \lambda \quad (1)$$

where  $n$  is an integer, is the condition for Constructive Interference.

At any location along the medium where the two superimposing waves have a path difference equal to half integral multiple of wavelength, the waves are set to interfere destructively. So,

$$\text{Path difference} = \left(n + \frac{1}{2}\right) \lambda \quad (2)$$

is the condition for destructive interference.

For observing interference, it is essential that the two superimposing waves have the same wavelength, frequency, velocity and a constant phase relationship.

### IV. SIMULATING INTERFERENCE EFFECTS

The interference effects can be demonstrated in the laboratory with ripples on the surface of water. Two pins are attached to the same prong of an electrically maintained tuning fork and adjusted so that the pins just touch the surface of water placed underneath, while the prongs are capable of vibrating in a vertical plane. The periodic vibratory motion of the prongs is taken up by the attached pins, which are, therefore always in equal phase. This periodic vibratory up and down motion of the pins, on the surface of water generates two waves or ripples systems of equal amplitude, equal wavelength and equal velocity. The ripples spread out with their centers at the points of action of two pins. In the present work, the above experimental setup has been simulated using **SCILAB**.

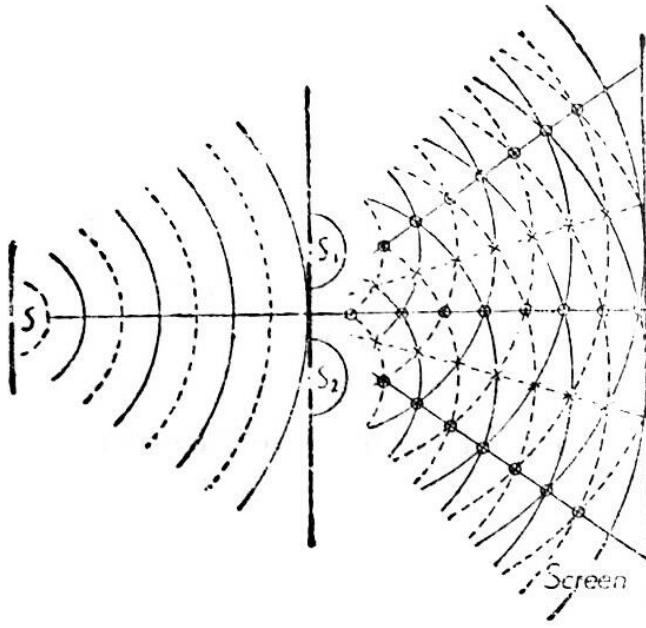


**Figure (2):** Schematic representation of spreading of ripples on the surface of water

The separation between the two pins is taken to be  $d$ . Each of the two pins act as a point source giving out circular wave fronts propagating in all directions. Thus, we get two sets of concentric circles, one centered at each of the two point sources. To simulate interference, the intersections of one set of concentric circles with a circle of given radius from the other set are found as follows:

Let  $S_1$  and  $S_2$  be the two point sources. With  $S_1$  as centre, a circle of radius  $r$  is chosen. If the plane containing  $S_1$  and  $S_2$ , i.e., the surface of water on which ripples are formed is taken to be the XY-plane with origin at  $S_1$ , then the equation of the circle is

$$x^2 + y^2 = r^2 \quad (3)$$

If Y-axis is along the line joining  $S_1$  and  $S_2$ , then the coordinates of  $S_2$  are  $(0, -d)$ . If P is an arbitrarily chosen point on the circle, then  $(S_2P - S_1P)$  can be taken to be the path difference between the two waves originating at the same instant from  $S_2$  and  $S_1$  respectively on reaching the point P. If

$$|S_2P - S_1P| = n\lambda, \quad (4)$$

the two waves interfere constructively, and if

$$|S_2P - S_1P| = \frac{(2n+1)\lambda}{2}, \quad (5)$$

the interference is destructive.

It can be easily seen that

$$S_1P = r \text{ and} \quad (6)$$

$$S_2P = \sqrt{x^2 + (y + d)^2} \quad (7)$$

This gives us, for constructive interference,

$$|S_2P - S_1P| = |\sqrt{x^2 + (y + d)^2} - r| = n\lambda \quad (8)$$

And for destructive interference,

$$|S_2P - S_1P| = |\sqrt{x^2 + (y + d)^2} - r| = \frac{(2n+1)\lambda}{2} \quad (9)$$

Rewriting equations (8) and (9) as,

$$\sqrt{x^2 + (y + d)^2} = \pm n\lambda + r \quad (10)$$

$$\sqrt{x^2 + (y + d)^2} = \pm \frac{(2n+1)\lambda}{2} + r \quad (11)$$

Squaring both sides of equations (10) and (11), we get,

$$x^2 + (y + d)^2 = (\pm n\lambda + r)^2 \quad (12)$$

$$x^2 + (y + d)^2 = \left(\pm \frac{(2n+1)\lambda}{2} + r\right)^2 \quad (13)$$

It is to be noted that equations (12) and (13) represent sets of concentric circles centered at  $S_2$  having radii determined by the value of  $n$ , the order of interference maxima and minima. Thus, we simulate the locations of constructive and destructive interference of waves by the points of intersection of these concentric circles with the circle of radius  $r$  centered at  $S_1$ .

## V. SCILAB SIMULATIONS

In the following simulations we consider the values of variables to be as follows:

Distance between point sources ( $d$ ) = 3cm  
 Radius of the circular wavefront ( $r$ ) = 5cm  
 Wavelength of the waves ( $\lambda$ ) = 1cm

We check the position of points of maxima and minima for different orders using simulations. The blue dot in Figure (3) represents the point source  $S_1$

and the red dot represents the point source  $S_2$ . The blue circle is the loci of all points at a definite radius ( $r=5\text{cm}$  in this simulation) from the point source  $S_1$ .

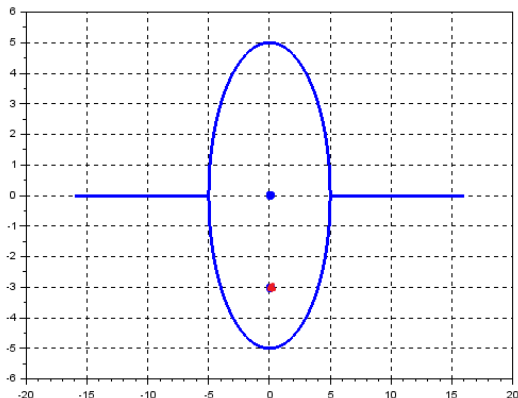


**Figure (3):** Two point sources and a circle having source  $S_1$  as its center.

The red and the black circles correspond to equations (12) and (13) representing loci of all points where maxima and minima occur respectively. In all the simulations, the intersection of the red circle with the blue circle gives the positions of maxima and the points of intersection of the black circle with blue circle gives the position of minima on the wave front of radius  $r$  that originated from the point source  $S_1$ .

The positions for different order maxima and minima are depicted in the following figures:

**Case (i):**  $n = 0$

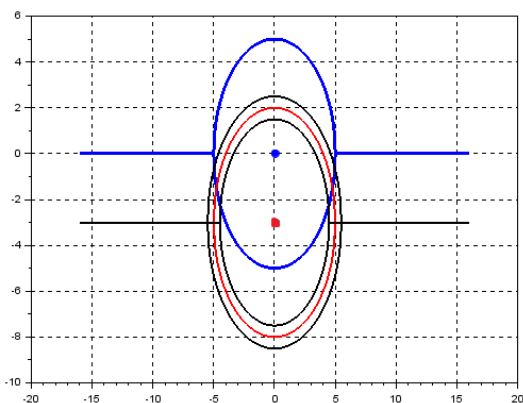


**Figure (4):** Two points of maxima and four points of minima for  $n = 0$ .

**Case (ii):**  $n = 1$

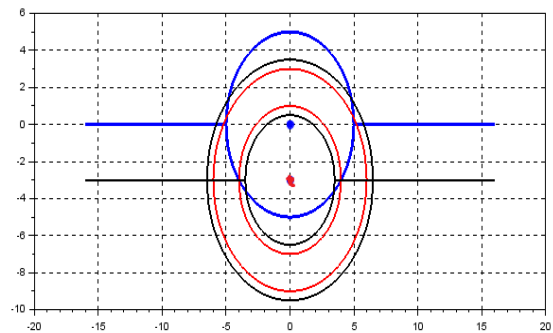


**Figure (5):** Four points of maxima and four points of minima for  $n = 1$ .

**Case (iii):**  $n = 2$

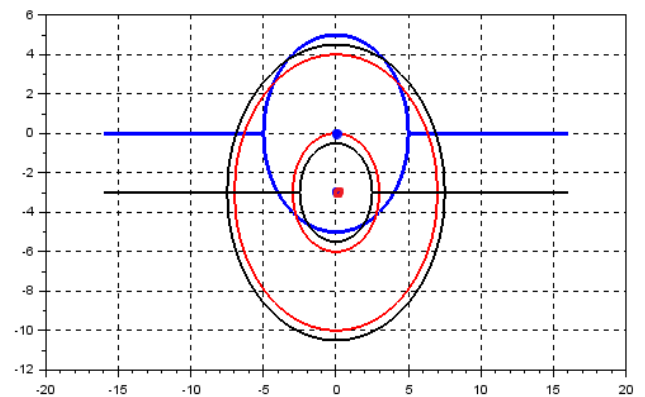


**Figure (6):** Four points of maxima and four points of minima for  $n = 2$ .

**Case (iv):**  $n = 3$

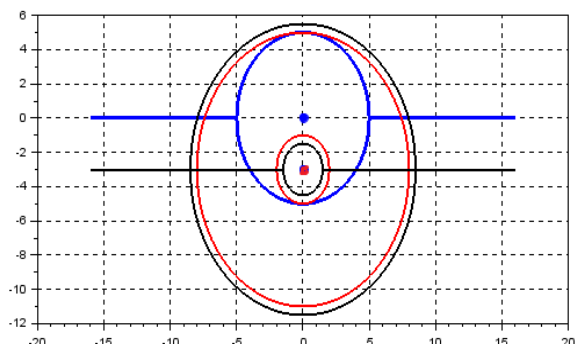


**Figure (7):** Two points of maxima and no minima for  $n=3$

**Case (v):  $n = 4$**

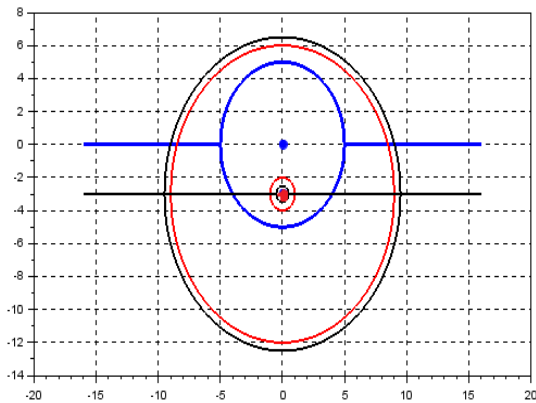


**Figure (8):** No points of maxima and minima for  $n = 4$ .

All the cases discussed above are clubbed in Figure 9.

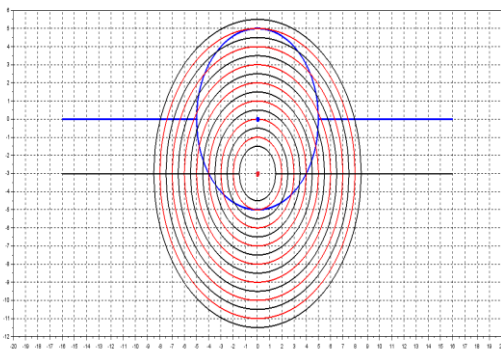


**Figure (9):** All the possible points of maxima and minima for a wave front from source  $S_1$  having radius  $r$ .

It depicts the points of maxima and minima of all the possible orders that can be observed together for a circle of definite radius.

In the following Figure 10, different wave fronts originating from  $S_1$  are represented by blue concentric circles of varying radii. The intersection of these circles, with red and black circles corresponding to wave fronts originating from the source  $S_2$  give the locations of maxima and minima respectively. The black dots represent the points of minima and the red dots represent points of maxima.

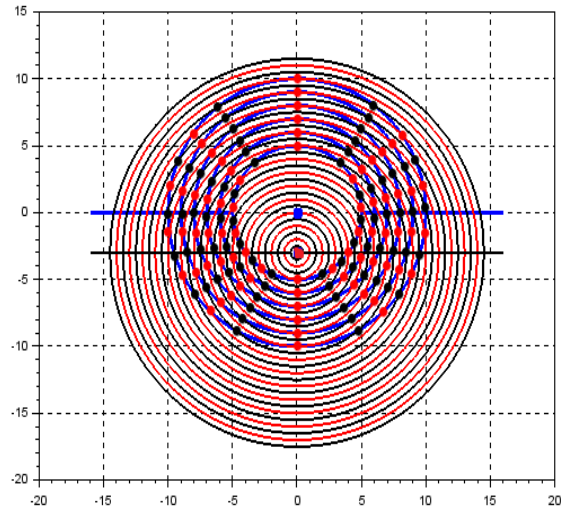


**Figure (10):** Representation of points of maxima and minima on wavefronts of different radii.

## VI. OBSERVATIONS AND DEDUCTIONS

From the above simulations using SCILAB, following observations and deductions can be made:

1. The maximum order of maxima and minima that can be observed depends on the ratio of distance ( $d$ ) between the sources and the wavelength ( $\lambda$ ) of the waves. If  $d/\lambda = k$ , then the maximum possible order of maxima would be an integer less than or equal to  $k$  and for minima, maximum possible order would be one less. The highest order of interference maxima and minima is independent of the radii of superimposing wave fronts.

- In the present case, irrespective of the radius of the circle, there are four points on the circle corresponding to a given order (with zeroth and the highest order being exceptions) of maxima and minima, one in each quadrant. For the zeroth order case, there are two points of maxima and four points of minima. For the highest order ( $n = 3$  in the present simulation), there are two maxima and no minima.
- The points of maxima and minima can be joined with opposite points lying on the other side of y-axis for the same value of ordinate by a chord parallel to x-axis (Figure 11). The maxima and minima for the same order do not necessarily lie diametrically opposite to each other (last case is an exception).

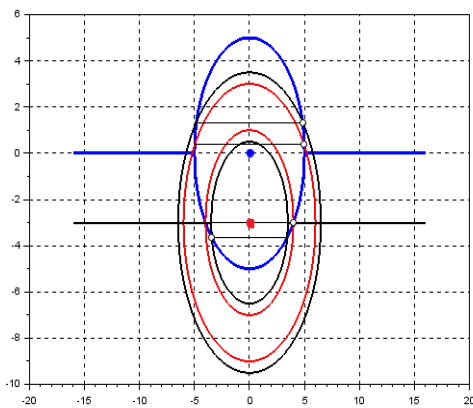


**Figure (11):** The chords joining the points of maxima and minima respectively on opposite side of y-axis

- From Figure (10), it can be seen that the points of maxima and minima are not equally spaced on a given wave front. However, the points of maxima and minima of a given order in each quadrant lie along a straight line.

## VII. YOUNG'S DOUBLE SLIT EXPERIMENT

Different observers can view at the same instant different objects through the same narrow aperture with perfect clarity, the beams of light having crossed at the aperture in reaching the observers. This establishes the validity of the superposition principle for light and hence, the principle can be

used in investigating the disturbance in regions where two or more light waves are superimposed. Historically, the phenomenon of 'Interference of light' was first discovered by Thomas Young in 1801. He performed an experiment exhibiting interference pattern due to the superposition of two beams of light, thus establishing the wave nature of light. This experiment is known to us as the famous Young's Double Slit Experiment.

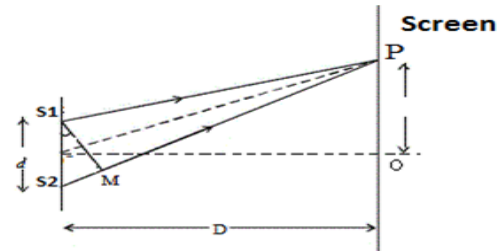


**Figure (12):** Schematic representation of Young's Double Slit experiment.

In the original experimental set-up, Young allowed the sun light to pass through a pin hole  $S$  and then at some distance through two sufficiently close pin holes  $S_1$  and  $S_2$  in an opaque screen. Finally, the light was received on a screen on which he observed an uneven distribution of light intensity. The illumination on the screen consisted of many alternate bright and dark spots. In accordance with the modern Laboratory technique narrow parallel slits replace pin-holes and the slit  $S$  is illuminated with monochromatic light of wavelength  $\lambda$ . Light is received on a screen placed at a certain distance from the plane containing the parallel slits  $S_1$  and  $S_2$ .

A schematic representation of the experimental set-up is given in the Figure 12.

The two slits  $S_1$  and  $S_2$  are taken to be along the z-axis having coordinates  $(0, 0, d/2)$  and  $(0, 0, -d/2)$  respectively. If  $P$  is the point of observation having coordinates  $(x, y, z)$ , then the path difference between the superimposing waves from  $S_1$  and  $S_2$ , on reaching  $P$  is given by

$$\Delta = S_2P - S_1P \quad (14)$$

$$\Delta = \sqrt{x^2 + y^2 + \left(z + \frac{d}{2}\right)^2} - \sqrt{x^2 + y^2 + \left(z - \frac{d}{2}\right)^2} \quad (15)$$

Equation (15) on simplification by squaring both sides gives

$$\frac{z^2}{\frac{\Delta^2}{4}} - \frac{x^2}{\frac{d^2-\Delta^2}{4}} - \frac{y^2}{\frac{d^2-\Delta^2}{4}} = 1 \quad (16)$$

which is the equation of a hyperboloid for a given value of  $\Delta$ .

An interference maxima occurs when  $\Delta = n\lambda$  and for minima  $\Delta = \frac{(2n+1)\lambda}{2}$ .

Hence, the shape of an interference fringe is given by the loci of points of constant  $\Delta$ , the path difference between the superimposing waves. In three dimensional space, this is a hyperboloid surface given by equation (16).

In our experimental set-up, we generally obtain interference pattern on a screen placed at a desired location with respect to the screen containing the pin holes  $S_1$  and  $S_2$ . The observation screen is simulated by a plane having the desired orientation. The intersection of this plane with the hyperboloid surface would give the shape of interference fringe on the screen. Simulations corresponding to screen oriented at angle  $\theta = 0, 30, 45$  and  $90$  Degrees to the line joining the slits are discussed in the following section.

### VIII. SHAPE OF FRINGES

The screen containing  $S_1$  and  $S_2$  is simulated by the XZ- plane in the present analysis.

#### Case (i): $\theta = 0^\circ$

The observation screen is parallel to the screen containing  $S_1$  and  $S_2$ . Let it be represented by the plane  $y=D$ , where  $D$  is an arbitrarily chosen constant. Substituting  $y=D$  in the equation of hyperboloid (equation 16), we get,

$$\frac{z^2}{\frac{\Delta^2}{4}} - \frac{x^2}{\frac{d^2-\Delta^2}{4}} = 1 + \frac{D^2}{\frac{d^2-\Delta^2}{4}} \quad (17)$$

which is the equation of a hyperbola in the  $y=D$  plane. Thus a hyperbolic fringe is obtained when the observation screen is placed parallel to the plane of the slits. This is shown in figure (13) below.

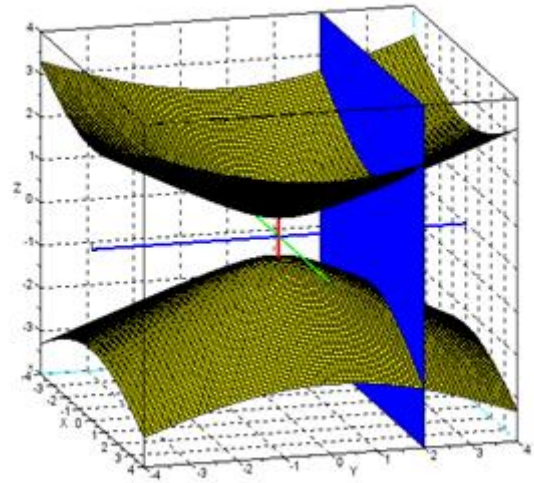


**Figure (13):** The observation screen is placed parallel to the plane of the slits

The green, blue and red axis denotes x, y, and z axis respectively. Yellow coloured shapes are the hyperboloids. The red axis is also the line joining the two slits. The blue plane is the screen which is placed at distance  $D$  from the plane of the slits. Figure (14) shows the view of the above from a different angle.

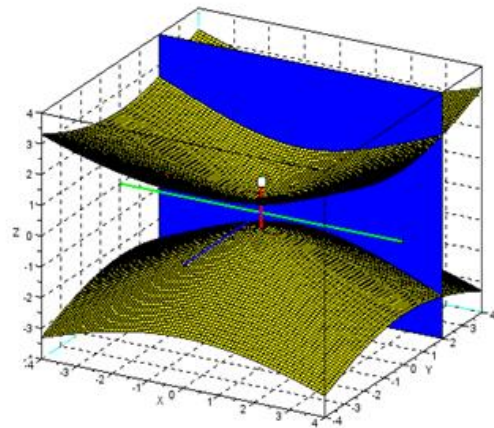


**Figure (14):** When viewed from a different angle

**Case (ii):  $\theta = 90^\circ$**

The observation screen is perpendicular to the line joining the two slits, i.e., the z-axis. Let it be represented by the plane  $z=D$ . Substituting this in the equation of hyperboloid (equation (16)) and rearranging the terms, we get,

$$x^2 + y^2 = \frac{4}{(d^2 - \Delta^2)} \left( \frac{D^2}{4} - 1 \right) \quad (18)$$

which is the equation of a circle in the XY-plane. Thus, the fringes are circular when obtained on a screen kept perpendicular to the line joining the two slits. These are shown in the figure (15) below. The observation screen is simulated the plane  $z=D$ .

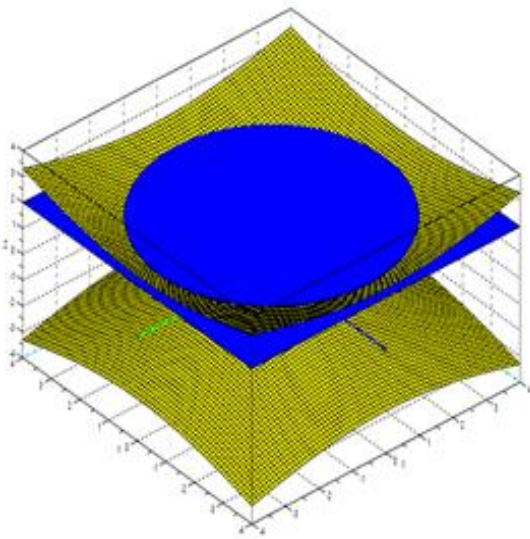


**Figure (15):** The observation screen is placed perpendicular to the line joining the two slits.

**Cases (iii) and (iv):  $\theta = 30^\circ$  and  $45^\circ$**

Figures (16) and (17) below simulate the hyperbolic fringes formed on screens oriented at angles  $30^\circ$  and  $45^\circ$  respectively with the line joining the slits, i.e., the z-axis.

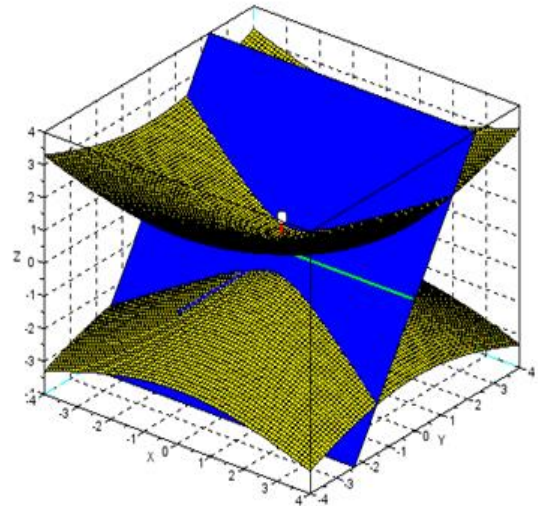


**Figure (16):** The screen is placed at  $30^\circ$  to the line joining the slits.

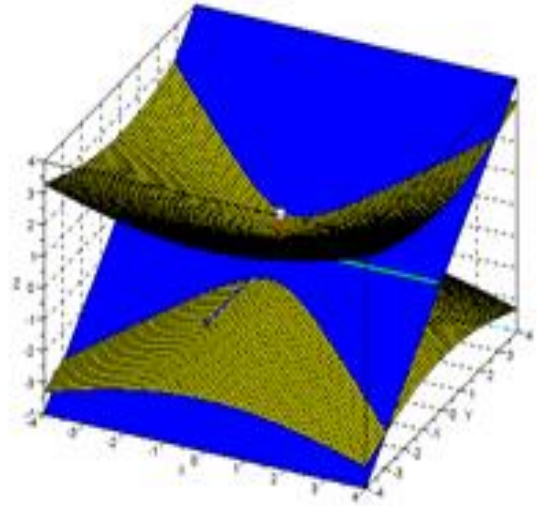


**Figure (17):** The screen is placed at  $45^\circ$  to the line joining the slits

**IX. DISCUSSION**

In each of the cases discussed so far,  $\Delta$  has been assigned one value giving a single hyperboloid surface, whose intersection with differently oriented planes is either a hyperbola or a circle. Physically, these represent hyperbolic or a circular interference fringe of a given order of maxima or

minima, corresponding to  $\Delta = n\lambda$  or  $\Delta = (2n+1)\lambda/2$  respectively, obtained on the screen. By assigning different integral values to  $n$ , the order of interference fringe, a series of hyperbolae or concentric circles are formed on the plane intersecting the multiple hyperboloid surfaces, corresponding to different values of  $\Delta$  as given by equation (16).

This is shown in Figures 18 and 19 for two different angles of view, when the plane is oriented parallel to the plane of the slits at a distance  $D$  from it. This simulates the interference pattern obtained on a screen kept parallel to the plane of the slits at a distance  $D$  in the physical experimental set-up.

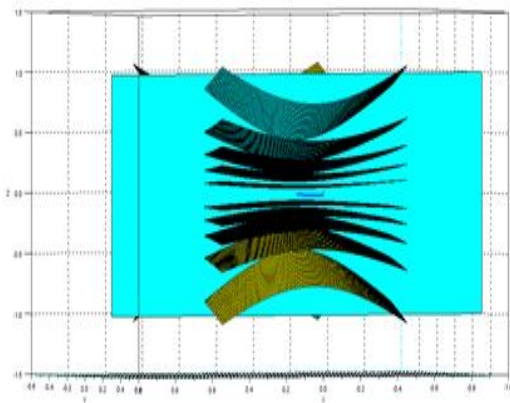


**Figure (18):** Multiple Hyperboloid surfaces corresponding to different values of  $\Delta$ . Intersection of these surfaces with a plane ( $y=D$ ) parallel to the plane of  $S_1$  and  $S_2$  (the XZ plane) giving a series of hyperbolae. In this simulation,  $D = 2\text{cm}$ ,  $d = 3\text{mm}$  and  $\lambda = 0.5\text{mm}$  is taken.

Furthermore, the projections of the slits  $S_1$  and  $S_2$  on a screen (simulated by  $y=D$  plane) will have coordinates  $(0, D, d/2)$  and  $(0, D, -d/2)$  respectively. These are the foci of the hyperbolic fringes formed on the screen. For observation points on the screen, we can put  $D=0$  in equation (17) and re-write the equation of hyperbola as,

$$\frac{z^2}{\frac{\Delta^2}{4}} - \frac{x^2}{\frac{d^2 - \Delta^2}{4}} = 1 \quad (19)$$

The eccentricities of these hyperbolae corresponding to different values of  $\Delta$  are given by

$$e = \sqrt{\frac{\Delta^2}{4} + \frac{d^2 - \Delta^2}{4}} \div \frac{\Delta}{2} = \frac{d}{\Delta} \quad (20)$$

In physical experimental set-ups for observing interference of light, the path difference  $\Delta$  corresponding to the condition of constructive or destructive interference is of the order of  $10^{-8}\text{cm}$  and  $d$  is of the order of  $10^{-2}\text{cm}$ . From equation (20) it can be seen that the eccentricities of the optical hyperbolic fringes is very large. As a consequence, these hyperbolic fringes are practically straight lines. This is perhaps the reason behind many of the text books describing the interference fringes formed in Young's Double Slit Experiment as straight fringes perpendicular to the line joining the two slits.

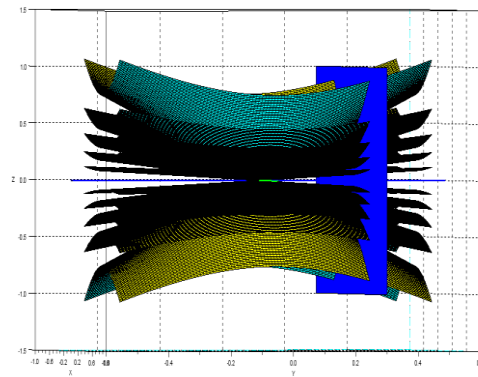


**Figure (19):** View from a different angle of the multiple Hyperboloid surfaces corresponding to different values of  $\Delta$ . Intersection of these surfaces with a plane parallel to the plane of  $S_1$  and  $S_2$  giving a series of hyperbolae.

## X. CONCLUSION

The step by step simulation of the phenomenon of interference of waves done in the present work is expected to aid the understanding of this very fundamental concept in physics by the students. More importantly, the exact hyperbolic shape of interference fringes formed in Young's Double Slit Experiment on interference of waves from two point sources or slits, which is never observed in any physical experimental set-up for observing interference of light, is however, simulated in the present work. This would ensure that the students know the actual shape of interference fringes and

why they observe only straight fringes in an optical experimental set up.

### REFERENCES

1. Fundamental of Optics; Francis A. Jenkins, Harvey E. White; McGraw Hill Book Company.
2. Principles of Optics; B.K. Mathur; (out of print)
3. S.Enterprises,"Home-Scilab",Scilab.org,2017.  
[Online]  
Available:<https://www.Scilab.org/>

# Young's Modulus using Wind Chimes

Shirish Pathare and Sharvani Shahapurkar  
Homi Bhabha Centre for Science Education,  
V. N. Purav Marg, Mankhurd. Mumbai - 400088  
shirish@hbcse.tifr.res.in

*Submitted on 01-01-2019*

## Abstract

Various experiments on determination of Young's modulus are part of undergraduate physics laboratory curriculum. Wind chimes, a musical instrument, can also be used to determine the Young's modulus [1]. In this paper we use an app on android device to capture and analyse the frequency of the note produced by the wind chimes.

Since the percussion instruments are struck according to the random effects of the wind blowing the chimes, wind chimes have been considered as an example of chance-based music. In this experiment, we determine the Young's modulus of the material of the pipe used in wind chimes. The Young's modulus depends on the frequency of the note produced. In order to capture and analyse this frequency, Forinash et. al. used a microphone with amplifying circuit in which voltages from the microphone were digitized using an analog-to-digital conversion board [1]. In this paper we have used a simpler method in which an android device app "Pano Tuner" (also available for iOS devices) detects the sound and displays its frequency.

## 1 Introduction



Figure 1:  
Wind  
Chimes

Wind chimes is a type of percussion instrument constructed from suspended tubes, rods, bells or other objects that are often made of metal or wood (figure 1). The tubes are suspended along with some type of weight or surface to which the tubes can strike when they are blown by the natural movement of air outside. You must have seen them hung at some residence.

## 2 Apparatus

6 aluminum pipes of different lengths, a black metal strip (with a magnet) attached to the retort stand, an allen key, a thread for hanging pipes, an acrylic pipe (for striking

the aluminum pipes), a vernier calipers, a 30.0 cm plastic scale, A digital weighing balance (least count = 0.1 g), a tablet with a software Pano Tuner.

### 3 Description of Apparatus

1. Aluminum pipes: Six Aluminum pipes of different lengths 12.0cm, 14.0cm,16.0cm, 18.0cm, 20.0cm, 22.0cm are used. The center of each pipe is marked (figure 2).



Figure 2: Six aluminum pipes with centers marked

The graph in figure 3 gives the first four modes in a vibrating cantilever beam. In this experiments we have considered the fundamental mode of vibration. In this mode the antinode is at the centre and the node is at a distance  $0.224L$  [2], where  $L$  is the length of the pipe. The pipe is, therefore, hung at the position of node (figure 4) and struck at the centre.

2. Black metal strip support: The black metal strip is provided to hang pipes of different length. One end of the thread can be held to the support using a magnet. The other end is to be tied to the pipe at a distance  $x$  (figure 4).

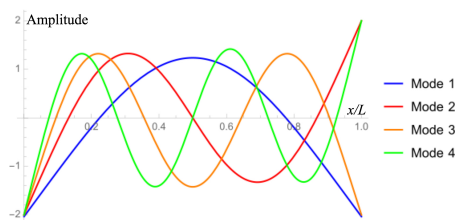


Figure 3: First four modes of vibrating free beam [3]

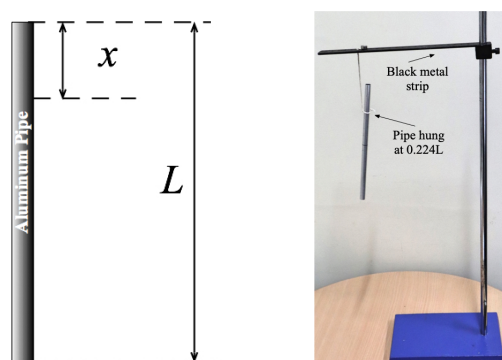


Figure 4: Pipe hanging at distance  $x$

3. Acrylic pipe: The acrylic pipe (figure 5) is provided to strike the aluminum pipe. Gently hit the aluminum pipe at center with this acrylic pipe to produce sound.



Figure 5: Acrylic pipe

4. Tablet: We used an android tablet. The Pano Tuner app (figure 6) is installed on the tablet. The app is a chromatic tuner and catches the note produced through its microphone and displays its frequency.
5. Producing sound: You are given



Figure 6: Pano tuner app

an acrylic pipe. Gently strike the aluminum pipe by the acrylic pipe. The aluminum pipe should always be struck at the center. Hold the microphone end of the tablet nearer to the pipe to pick up the note produced (figure 7).



Figure 7: Producing sound

#### 4 Theory

The speed of sound in aluminum is  $v_{Al}$ , expressed as

$$v_{Al} = \frac{8f}{9\pi KL^n}$$

where,  $f$  is the frequency of sound produced by pipe when struck,  $L$  is the length of the pipe,  $K$  is the radius of gyration for a pipe ( $\frac{1}{2}\sqrt{a^2 + b^2}$ ),  $a$  and  $b$  are the inner and outer radii of the pipe,  $n$  is an integer. Further the

speed of sound in a metal is also expressed in terms of the Youngs modulus  $Y$  and the density of the metal  $\rho$  as

$$v = \sqrt{\frac{Y}{\rho}}$$

#### 5 Experiment

1. Determine  $n$  by plotting a suitable graph and rewrite the expression of  $v_{Al}$  on substituting  $n$ .
2. Determine the speed of sound in aluminum by plotting a suitable graph. Calculate standard uncertainty in the speed of sound in aluminum.
3. Determine the density of aluminum by plotting a suitable graph. Calculate the standard uncertainty in the density.
4. Determine the Youngs modulus of aluminum,  $Y$  with standard uncertainty in  $Y$ .

#### 6 Observations and Calculations

In this section we present the data collected using the wind chimes assembly described above. We begin with the measurement of inner and outer radii. Then the frequency of the note produced by each pipe is captured using the Pano Tuner app. Mass ( $m$ ) of each aluminum pipe was measured using digital weighing pan (with its least count equal to 0.1 g) and then the density of each pipe is calculated.

**Determination of inner and outer radius:**

Pipe length = 22.0 cm				
$2a_1/cm$	$2a_2/cm$	$2a_3/cm$	<i>Mean a/cm</i>	$\Delta a/cm$
0.782	0.780	0.778	0.390	0.001
$2b_1/cm$	$2b_2/cm$	$2b_3/cm$	<i>Mean b/cm</i>	$\Delta b/cm/cm$
0.900	0.896	0.902	0.450	0.002

Pipe length = 20.0 cm				
$2a_1/cm$	$2a_2/cm$	$2a_3/cm$	<i>Mean a/cm</i>	$\Delta a/cm$
0.774	0.768	0.766	0.385	0.002
$2b_1/cm$	$2b_2/cm$	$2b_3/cm$	<i>Mean b/cm</i>	$\Delta b/cm/cm$
0.898	0.898	0.894	0.448	0.001

Pipe length = 18.0 cm				
$2a_1/cm$	$2a_2/cm$	$2a_3/cm$	<i>Mean a/cm</i>	$\Delta a/cm$
0.768	0.772	0.772	0.385	0.001
$2b_1/cm$	$2b_2/cm$	$2b_3/cm$	<i>Mean b/cm</i>	$\Delta b/cm/cm$
0.892	0.892	0.892	0.446	0.001

Pipe length = 16.0 cm				
$2a_1/cm$	$2a_2/cm$	$2a_3/cm$	<i>Mean a/cm</i>	$\Delta a/cm$
0.780	0.778	0.778	0.390	0.001
$2b_1/cm$	$2b_2/cm$	$2b_3/cm$	<i>Mean b/cm</i>	$\Delta b/cm/cm$
0.902	0.898	0.900	0.450	0.001

Pipe length = 14.0 cm				
$2a_1/cm$	$2a_2/cm$	$2a_3/cm$	<i>Mean a/cm</i>	$\Delta a/cm$
0.768	0.774	0.774	0.386	0.002
$2b_1/cm$	$2b_2/cm$	$2b_3/cm$	<i>Mean b/cm</i>	$\Delta b/cm/cm$
0.898	0.900	0.900	0.450	0.001

Pipe length = 12.0 cm				
$2a_1/cm$	$2a_2/cm$	$2a_3/cm$	<i>Mean a/cm</i>	$\Delta a/cm$
0.770	0.774	0.774	0.386	0.001
$2b_1/cm$	$2b_2/cm$	$2b_3/cm$	<i>Mean b/cm</i>	$\Delta b/cm/cm$
0.894	0.894	0.892	0.447	0.001

$$a \pm \Delta a = 0.387 \pm 0.004 \text{ cm}$$

$$b \pm \Delta b = 0.449 \pm 0.003 \text{ cm}$$

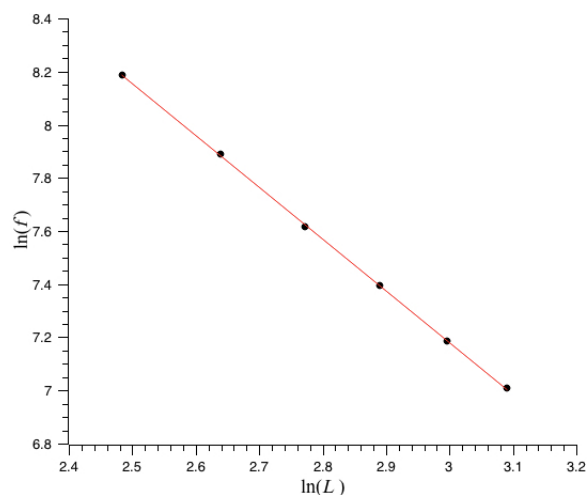
No.	L /cm	x /cm
1	22.0	4.9
2	20.0	4.5
3	18.0	4.0
4	16.0	3.6
5	14.0	3.1
6	12.0	2.7

Frequency detected using Pano Tuner app:

No.	L /cm	f <sub>1</sub> /Hz	f <sub>2</sub> /Hz	f <sub>3</sub> /Hz	f <sub>4</sub> /Hz	f <sub>5</sub> /Hz	Mean f /Hz
1	22.0	1107.0	1108.1	1107.2	1108.2	1108.3	1107.8
2	20.0	1316.0	1320.2	1317.9	1320.0	1316.8	1318.2
3	18.0	1628.2	1627.9	1629.3	1627.2	1629.2	1628.4
4	16.0	2032.8	2038.0	2032.4	2035.0	2033.2	2034.3
5	14.0	2667.2	2661.9	2659.8	2666.5	2681.2	2667.3
6	12.0	3587.3	3592.2	3594.4	3595.1	3592.2	3592.2

**Determination of n:**

No.	L /cm	f /Hz	ln(L)	ln(f)
1	22.0	1107.8	3.091	7.010
2	20.0	1318.2	2.996	7.184
3	18.0	1628.4	2.890	7.395
4	16.0	2034.3	2.773	7.618
5	14.0	2667.3	2.639	7.889
6	12.0	3592.2	2.485	8.187



Slope of the graph = -1.95

$$\therefore n = -2$$

Figure 8: Graph of  $\ln(f)$  against  $\ln(L)$

Therefore the expression for  $v_{Al}$  is:

$$v_{Al} = \frac{8fL^2}{9\pi K}$$

**Determination of  $v_{Al}$ :**

No.	$L / \text{cm}$	$1/L^2 / \text{m}^{-2}$	$f / \text{Hz}$
1	22.0	20.66	1107.8
2	20.0	25.00	1318.2
3	18.0	30.86	1628.4
4	16.0	39.06	2034.3
5	14.0	51.02	2667.3
6	12.0	69.44	3592.2

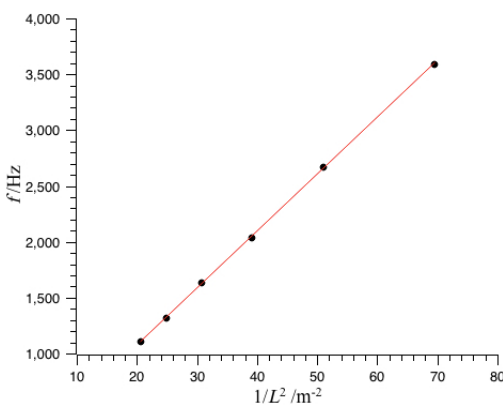


Figure 9: Graph of  $f$  against  $1/L^2$

Slope of the graph =  $51.11 \text{ Hz.m}^2$

$$v_{Al} = \frac{8fL^2}{9\pi K} = \frac{16 \times 51.11}{9\pi \sqrt{(0.387^2) + (0.449^2)}}$$

Thus the value of speed of sound in aluminum is

$$v_{Al} = 4881 \pm 18 \text{ m/s.}$$

**Determination of density:**

No.	$L / \text{cm}$	$m / \text{g}$
1	22.0	8.8
2	20.0	8.1
3	18.0	7.3
4	16.0	6.5
5	14.0	5.7
6	12.0	4.8

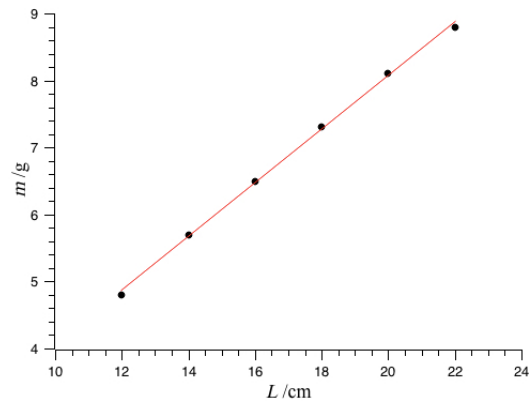


Figure 10: Graph of mass against length

Slope of the graph =  $0.4 \text{ g/cm}$

Density of aluminum:

$$\text{Density} = \frac{m}{V} = \frac{m}{\pi(b^2 - a^2)L} = \frac{\text{Slope}}{\pi(b^2 - a^2)}$$

$$\text{Density} = 2.46 \pm 0.04 \text{ g.cm}^{-3}.$$

**Determination Young's modulus:**

$$v = \sqrt{\frac{Y}{\rho}} = \sqrt{\frac{Y}{2458}} = 4881 \text{ m/s}$$

$$Y = 59 \pm 1 \text{ GPa}$$

**Young's modulus of other metals:**

The experiment was also carried out for copper and brass pipes of different dimensions and their Young's Modulus was determined.

	Copper	Brass
$a / \text{cm}$	$0.527 \pm 0.002$	$0.533 \pm 0.002$
$b / \text{cm}$	$0.738 \pm 0.002$	$0.713 \pm 0.002$
$L / \text{cm}$	$25.4 \pm 0.1$	$25.6 \pm 0.1$
$m / \text{g}$	$178.1 \pm 0.1$	$139.6 \pm 0.1$
$f / \text{Hz}$	$914 \pm 1$	$899 \pm 1$
$v \text{ m/s}$	$3686 \pm 24$	$3748 \pm 23$
$\rho \text{ g/cm}^3$	$8.37 \times 10^3$	$7.74 \times 10^3$
$Y \text{ GPa}$	$114 \pm 4$	$109 \pm 2$
$Y \text{ GPa [4]}$	117	102 - 125

The literature values for the Young's modulus of these metals are given in the last row which matches with the values obtained from the experiment.

## 7 Conclusion

In this paper we have used a simple method to determine the Young's modulus of material of different metals. The android device with the app Pano Tuner gives consistent values of frequency of the note produced by the wind chime. The apparatus required in this experiment is commonly available. Very simple measurements lead to fairly accurate values of Young's modulus. All these reasons make this experiment suitable at the undergraduate level.

## Acknowledgments

We would like to thank the physics olympiad program of the Homi Bhabha Centre for Science Education for funding

our work. We would like to thank our colleagues at HBCSE and from different colleges in the country who helped us in standardizing the apparatus. Lastly we would like to thank all the students who performed this experiment in the camp.

## References

- [1] Forinash K., Richie Jr. J, Jones, T. (1990). Wind chime physics, Am. J. Phys,58(1),82
- [2] Rossing T. D., (2005) Science of Percussion instruments, World Scientific, Singapore, 48.
- [3] The first four modes of a vibrating free-free Euler-Bernoulli beam [https://en.wikipedia.org/wiki/EulerBernoulli\\_beam\\_theory](https://en.wikipedia.org/wiki/EulerBernoulli_beam_theory)
- [4] The engineering toolbox, [https://www.engineeringtoolbox.com/young-modulus-d\\_417.html](https://www.engineeringtoolbox.com/young-modulus-d_417.html)

# Market Analysis Using Three State Ising Model

Lisha Damodaran <sup>\*1</sup>, K. M. Udayanandan <sup>†2</sup>

<sup>1</sup> School of Pure and Applied Physics, Department of Physics  
Kannur University,  
Kerala- 670 327, INDIA

<sup>2</sup> Nehru Arts and Science College, Kanhangad  
Kerala- 671 314, INDIA  
udayanandan@gmail.com

*Submitted on 17-10-2018*

## Abstract

The Ising model which was introduced to explain ferromagnetism in physics provides a general background to build realistic models of social interactions. Here we use the thermodynamic study of a financial market using Ising model in which agents have three opinions (buy, sell or hold).

Key words: Econophysics, Thermodynamics, Ising model

[1, 2]. Among the various statistical models proposed, the Ising model and its variants [3, 4] played an important role in understanding the origin of the so-called stylized facts in real financial markets. A large set of economic models can be mapped onto various versions of the Ising model to account for social influence in individual decisions. Any marketplace that allows agents or traders to buy or sell financial goods such as bonds, currencies, stocks etc, is called a financial market. Financial markets are well defined complex systems, which are continuously monitored. Virtually every economic transaction is recorded, and the recorded economic data are becoming accessible to interested researchers. Facts such as these make financial markets extremely attractive for researchers interested in developing a deeper understanding of modeling of complex systems. In this paper we study the dependence of economic disorder in a financial

## 1 Introduction

Econophysics studies economic phenomena by using models and concepts imported from condensed matter and statistical physics. This new branch of economics represents a new template which aims to reinvent modern financial economic theory

market on the average money per agent and the interaction among the agents by making use of the concept of entropy and temperature and assuming that the system as a closed one. We use the three state Ising model to obtain the expression for money in this closed economic system. The economic quantities like average value of money and economic capacity are studied analogous to internal energy and heat capacity. A comparison is made using two state model [5] without external influence also.

## 2 Ising model

The Ising model, introduced initially as a mathematical model of ferro magnetism in statistical mechanics, is now part of the common culture of physics as the simplest representation of interacting elements with a finite number of possible states. The model consists of a large number of magnetic moments (or spins) connected by links within a graph, network or grid. Each spin interacts with its direct neighbors, tending to align together in a common direction, while the temperature tends to make the spin orientations random [3].

### Ising model in Physics

In one dimensional Ising model we consider  $N$  lattice sites arranged as a ring. Associated with each lattice there is a spin variable  $\sigma_i (i = 1, 2, 3, \dots, N)$  which can take either  $\pm 1$  or  $0$ . In order to avoid end effects, the periodic boundary condition is assumed

$$\sigma_{N+1} = \sigma_1 \text{ [6].}$$

The Hamiltonian in the absence of external field is given by

$$E(\sigma_i) = -J \sum_{i=1}^N \sigma_i \sigma_{i+1} \quad (1)$$

where  $J$  is the coupling coefficient. From  $E$  we get partition function

$$Q_N = \sum_{\text{overall states}} e^{-\beta E(\sigma_i)} \quad (2)$$

Free energy is defined as

$$F = -k_B T \ln Q_N \quad (3)$$

where  $k_B$  is Boltzmann constant and  $T$ , the temperature. The internal energy  $U$  is related to free energy as

$$F = U - TS \quad (4)$$

where  $S$  is the entropy. The thermodynamic quantities like entropy and specific heat capacity can be obtained [6] from the free energy using the expressions

$$S = - \left( \frac{\partial F}{\partial T} \right)_{N,V} \quad (5)$$

$$C = T \left( \frac{\partial S}{\partial T} \right)_{N,V} \quad (6)$$

A phase transition is always associated with discontinuities in the thermodynamic variables or its derivatives. The heat capacity can be used to show the existence of second order phase transition. In statistical mechanics a phase transition occurs in the limit  $T \rightarrow T_c$ , where the heat capacity diverges.

### 3 Ising model in Economics

Let us think of an economic activity to be composed of a large number of pairwise exchanges between agents. The economic agents may be individuals or corporations. In any such asset exchange, one receives some goods or service from each other. If we concentrate only on the cash exchanged, every trade is asset conserving [7]. The conservation law of money reflects its fundamental property that, unlike material wealth, money is not allowed to be manufactured by regular economic agents, but can be transferred between agents [8]. In a closed economic system, the total amount of money  $M$  is conserved. In real economic systems, the total number of agents is very large so that for many applications  $N \rightarrow \infty$  is appropriate like statistical systems. The amount of money  $m$  that an agent can earn depends on several additional parameters  $\lambda_1, \lambda_2, \lambda_3, \dots, \lambda_l$  called microeconomic parameters [8]. In order to have  $m(\lambda)$ , it is required to know the very specific conditions and relationships within an economic system. First we have to identify the conserved quantity, money, in terms of microeconomic parameters that influences capacity of an individual agent, then represent this relation mathematically so that  $m$  becomes a well defined function of  $\lambda$ . In this work we used energy equivalent expression for money from Ising model and hence from  $m(\lambda)$  we calculate the partition function  $Q(T)$  [8, 9].

In our model, we consider  $N$  agents placed on a one dimensional lattice with pe-

riodic boundary conditions same as used in Ising model. This geometry is taken in order to have simple and specific way of determining who is interacting with whom. The amount of money  $M$  can be written as

$$M = -C'_0 \sum_{i,j} \lambda_i \lambda_j$$

We take money per agent as

$$m = -C_0 \sum_{i,j} \lambda_i \lambda_j \quad (7)$$

here  $C'_0/N$  is the factor determining the interaction between agents. If we use two types of interaction **buy or sell** then the parameters  $\lambda_i, \lambda_j$  can take two states  $+1$  (buy state) and  $-1$  (sell state) and if we use three types of interaction **buy, sell and hold ( or do nothing)** then the parameters  $\lambda_i, \lambda_j$  can take three states  $+1$  (buy state),  $-1$  (sell state) and  $0$  (hold or do nothing). Then we have the partition function,

$$Q_N = \sum_{\text{overallstates}} e^{-m(\lambda)/T} \quad (8)$$

where  $T$  is the economic temperature which is the average amount of money per agent. Different countries have different economic temperatures. The difference of money temperatures between different countries allows one to extract profit in international trade. In this process, money (the analog of energy) flows from the high-temperature to the low-temperature country, in agreement with the second law of thermodynamics [9]. The partition function can be obtained using transfer matrix

method. A new quantity 'free money' similar to free energy is defined as [8]

$$F = -T \ln Q(T) \tag{9}$$

Similar to internal energy average value of money is defined as

$$\langle m \rangle = F + TS$$

Hence the economic entropy which is a measure of disorder in the market is,

$$S = - \left( \frac{\partial F}{\partial T} \right)_N \tag{10}$$

The economic capacity can be defined as

$$C = T \left( \frac{\partial S}{\partial T} \right)_N \tag{11}$$

At a particular economic temperature the divergence of  $c$  indicates the phase transition where the mean value of the money raises and the economic system undergoes a drastic change with agents possessing more and more money. However, this must end at some stage because of the fact that the total amount of money in the system is fixed and finite.

### 3.1 Market analysis using three state model

If we use three options in the interaction **buy, sell and hold ( or do nothing)** then the parameters  $\lambda_i, \lambda_j$  can take three states +1 (buy state), -1 (sell state) and 0 (hold or do nothing). Then we get partition function using Eq. 7. as,

$$\begin{aligned} Q_N &= \sum_{\text{overallstates}} e^{\frac{C_0 \sum_{ij} \lambda_i \lambda_j}{T}} \\ &= \sum_{\text{overallstates}} e^{\frac{C_0 \lambda_1 \lambda_2}{T}} e^{\frac{C_0 \lambda_2 \lambda_3}{T}} \dots e^{\frac{C_0 \lambda_N \lambda_1}{T}} \\ &= \text{Tr}(P^N) \end{aligned}$$

where  $P$  is the transfer matrix which is given by

$$P = \begin{pmatrix} e^{\left(\frac{C_0}{T}\right)} & 1 & e^{\left(-\frac{C_0}{T}\right)} \\ 1 & 1 & 1 \\ e^{\left(-\frac{C_0}{T}\right)} & 1 & e^{\left(\frac{C_0}{T}\right)} \end{pmatrix}$$

If  $x_1, x_2$  and  $x_3$  represent the eigen values, then

$$Q_N = x_1^N + x_2^N + x_3^N$$

The eigen values can be obtained by taking  $|P - xI| = 0$ . and solving,

$$x_1 = 2 \sinh \frac{C_0}{T} \tag{12}$$

$$x_2 = \frac{1}{2} [1 + 2 \cosh(C_0/T) + X] \tag{13}$$

$$x_3 = \frac{1}{2} [1 + 2 \cosh(C_0/T) - X] \tag{14}$$

where

$$X = \sqrt{8 + (2 \cosh(C_0/T) - 1)^2} \tag{15}$$

From the eigen values it is found that

$$x_2 > x_1 > x_3$$

Then,

$$Q_N = x_2^N = \left[ \frac{1}{2} [1 + 2 \cosh(C_0/T) + X] \right]^N \quad (16)$$

The free money per agent ( $f = F/N$ ) is given by,

$$f = -T \ln \left[ \frac{1}{2} [1 + 2 \cosh(C_0/T) + X] \right] \quad (17)$$

From  $f$  entropy is obtained as,

$$S = \ln \left[ \frac{1}{2} [1 + 2 \cosh(C_0/T) + X] \right] - \frac{T(4 \sinh(C_0/T))}{1 + 2 \cosh(C_0/T) + X} + \frac{[4((2 \cosh(C_0/T) - 1) \sinh(C_0/T))]}{T^2 X(1 + 2 \cosh(C_0/T) + X)}$$

The variation of economic entropy with economic temperature and interaction is shown in Figure 1. The average value of money is obtained as

$$\langle m \rangle = T^2 \frac{(4 \sinh(C_0/T))}{1 + 2 \cosh(C_0/T) + X} + \frac{[4((2 \cosh(C_0/T) - 1) \sinh(C_0/T))]}{X(1 + 2 \cosh(C_0/T) + X)} \quad (18)$$

### 3.2 Thermodynamics of money in two state model

For a comparison we use two states of the agents as either buy or sell, without external influence  $\lambda_i = +1$  for buy state and  $\lambda_i = -1$  for sell state. The partition function without external field [5] is obtained as,

$$Q_N = 2 \cosh \left( \frac{C_0}{T} \right) \quad (19)$$

The free money, entropy, average value of money and capacity are given below.

$$f = -T \ln \left[ 2 \cosh \left( \frac{C_0}{T} \right) \right] \quad (20)$$

$$S = \frac{C_0}{T} \tanh \left( \frac{C_0}{T} \right) + \ln \left[ 2 \cosh \left( \frac{C_0}{T} \right) \right] \quad (21)$$

$$\langle m \rangle = \frac{C_0}{T} \tanh(C_0/T) \quad (22)$$

The graphs showing entropy, average value of money and economic capacity for three state and two state models with economic temperature and interaction are shown in Figures 1, 2, 3, 4 and 5.

## 4 Discussions

Variation of entropy with economic temperature and interaction among the agents for three state and two state models are similar. It is seen that for low economic temperatures there is minimum entropy but as the temperature increases it increases and attains steady value. If the money per agent is more there will be more disorder in the market which indicates active state in the market. If the agents decide to hold or do nothing, the change will be gradual, but once it starts to decrease it is similar to the two state model. The entropy in financial systems depends on the states of interactions among agents, as interaction increases the entropy decreases. Here also three state model shows a slow variation with respect to the two state model. It is found that the

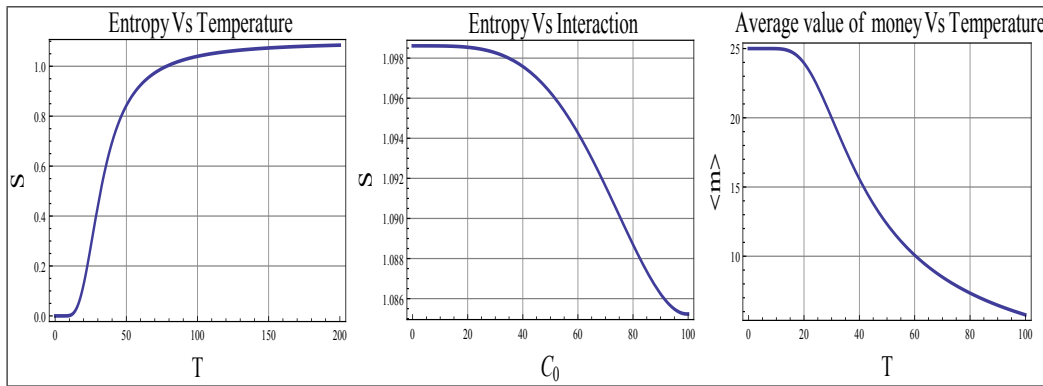


Figure 1: Three State model

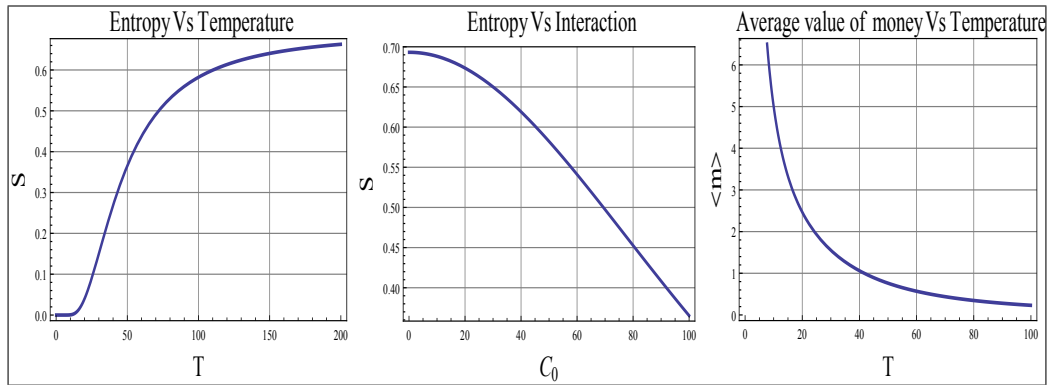


Figure 2: Two State model

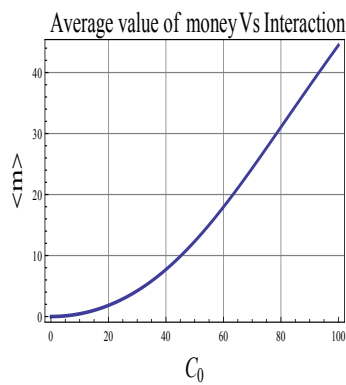


Figure 3: Three state model

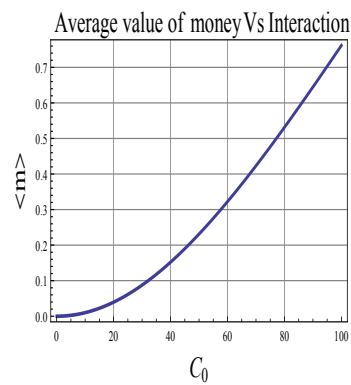


Figure 4: Two state model

average value of money remains constant for low economic temperatures and found to decrease as temperature increases, This in-

dicate that as the money per agent increases there is a chance of inflation which decreases the average value of money. When there

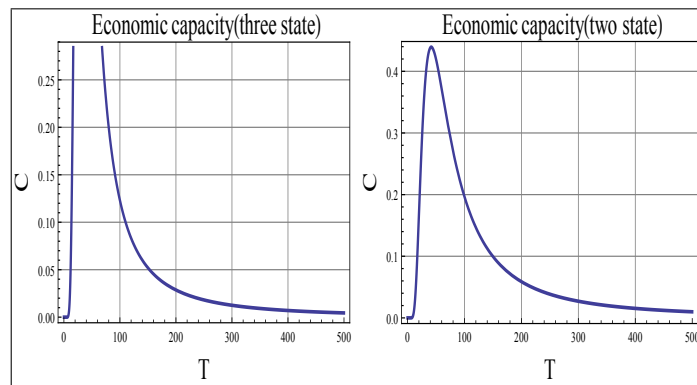


Figure 5: Capacity Vs interaction (Three and Two State model)

is maximum interaction between the agents the effect on the average value of money similar for the two models (Fig. 3 and 4). In Fig. 5, economic capacity shows a discontinuity at an economic temperature near zero which is an indication of transition which brings about a drastic change in the economic system. The capacity value was negative before this transition which is an indication of unstable state and then after transition changes to a positive value which shows that it is a stable state. If the agents decide to hold, the situation is more complex.. Such decisions create an unpredictable situation in the market in which the capacity of the market is not known. From this comparison we infer that the three state model of market is more close to the real nature of the market.

## 5 Conclusion

Here we use the thermodynamic equivalence of economic system. We consider Ising model as an economic model and study

the properties like entropy, average value of money, economic capacity against temperature and interaction strength. We found that economic temperature is a measure of sound economic systems. Using the plots we tried to predict the nature of the economic system by taking into account the interaction among the different economic agents. The phase transition nature is shown as a discontinuity in economic capacity. We suggest that certain models are needed for the real economic systems, so that one can study the properties of markets. This can be extended by considering next nearest agent interaction also. Here we have used Ising Hamiltonian without external field so if we consider the external field we can incorporate the effect of external influences and hence study the phase transition similar to magnetic transitions which will be discussed in our future work. This method provides flexibility which enhances the adaptation to real systems.

## Acknowledgement

Lisha Damodaran wishes to acknowledge the University Grants Commission for the assistance given under the Faculty Development Programme.

## References

- [1] Rosario N. Mantegna, H. Eugene Stanley, *An Introduction To Econophysics, Correlations and Complexity in Finance*, Cambridge University Press, (2000).
- [2] Franck Jovanovic And Christophe Schinckus, *Econophysics: A New Challenge For Financial Economics ?*, *Journal of the History of Economic Thought*, 35(03), 319 - 352, (2013).
- [3] Didier Sornette, *Physics and financial economics (1776-2014): puzzles, Ising and agent-based models*, *Rep. Prog. Phys.* 77, 062001, 28, (2014).
- [4] Phan D., Gordon M.B., Nadal J P., *Social Interactions in Economic Theory: An Insight from Statistical Mechanics*. In: Bourguine P., Nadal JP. (eds) *Cognitive Economics*. Springer, Berlin, Heidelberg, (2004).
- [5] Lisha Damodaran and K. M. Udayanandan, *Dynamics Of Stock Market Using Ising Model*, *Hyperion International Journal Of Econophysics & New Economy*, vol 11, Issue 1, 71-78, (2018)
- [6] R. K. Pathria and Paul D. Beale, *Statistical Mechanics*, Third Edition, Butterworth, (2011).
- [7] J. Dooyne Farmer, Martin Shubik, and Eric Smith, *Is Economics the Next Physical Science*, *Physics Today*, September (2005).
- [8] S. Prabhakaran, *Statistical Thermodynamics of Money (Thermoney)*, *International Journal of Applied Engineering Research*, 11(5), 3409-3420, (2016).
- [9] A. Drgulescu and V. M. Yakovenko, *Statistical mechanics of money*, *Eur. Phys. J. B* 17, 723-729, (2000).

# Exploring the non-linear Oscillations by means of the Law of Energy Conservation: two examples

V. Ivchenko

Department of Natural Sciences Training, Kherson State Maritime Academy,  
Kherson 73000, Ukraine.

reterty@gmail.com

*Submitted on 15-10-2018*

## Abstract

We consider the usefulness of the law of energy conservation in describing the non-linear oscillations. We show how to apply this fundamental law for finding and constructing amplitude, period, and phase portrait in the case of asymmetric non-linear oscillations. Two illustrative examples from electrostatics and molecular physics are analysed. These findings will be useful to the students, who study the oscillation phenomena.

## 1 Introduction

The idea of non-linearity is one of the key ideas of modern physics [1]. The non-linear approach to the analysis of physical theory is determined by its consistency, which most deeply and fully finds its theoretical reflection in the dialectics of the contradictory nature of things (the dialectics of the "linear" and "non-linear" nature of physical laws). The development of science, based on

the study of the phenomena of a new class of complexity, i.e. the non-linear systems and processes, leads to the development of deeper methods of scientific analysis and actually causes the emergence of a new vision of the World. The "non-linear thinking" is confirmed. The development of this kind of thinking should be continued throughout life, starting at the student level.

One of the broadest classes of the non-linear phenomena in physics is the non-linear oscillations [2]. The analysis of such oscillations is rather complicated and in principle requires knowledge of exact solutions of the equation of motion. However, some characteristics of these oscillations can be determined without finding the exact solutions by using only the law of conservation of energy.

Let us consider, as an example, the case of one-dimensional asymmetric non-linear oscillations, i.e. case of an asymmetric potential well  $V(x)$ . The minimum of this well corresponds to the stable equilibrium posi-

tion ( $x = 0$ ) of the system. The law of energy conservation has form:

$$\frac{m\dot{x}^2}{2} + V(x) = \text{const.} \quad (1)$$

Let  $A_+ > 0$  and  $A_- > 0$  be the amplitudes of the oscillation for  $x > 0$  and  $x < 0$  respectively. If we know the value of  $A_+$ , then using Eq. (1) we can write the following equation for finding the value of  $A_-$ :

$$V(-A_-) = V(+A_+). \quad (2)$$

Since  $\dot{x} = dx/dt$ , we derive from Eq. (1):

$$T_{\pm} = 2\sqrt{\frac{m}{2}} \int_0^{A_{\pm}} \frac{dx}{\sqrt{V(\pm A_{\pm}) - V(\pm x)}}. \quad (3)$$

Here  $T_+$  and  $T_-$  are the total time of motion within the one oscillation period  $T$  for  $x > 0$  and  $x < 0$  respectively. Naturally

$$T = T_+ + T_-. \quad (4)$$

Using Eq. (1) we can also construct a phase portrait of oscillations, which is the set of curves in the plane  $(x, \dot{x})$  for each of them the mechanical energy remains constant. The phase portraits are an invaluable tool in studying dynamical systems. In this paper we consider two illustrative examples of using Eqs. (2-4) in the analysis of non-linear oscillations.

## 2 The oscillations of a charged particle in the electrostatic field

The point particle with mass  $m$  and charge  $q$  can move along the line connecting two

fixed point charges  $q_-$  and  $q_+$ , wherein all three charges have the same sign:  $\text{sgn}(q) = \text{sgn}(q_-) = \text{sgn}(q_+)$  [3]. Using Coulomb's law we obtain the relation for distances  $l_- > 0$  and  $l_+ > 0$  (see Fig. 1) which define the equilibrium position of  $q$ :

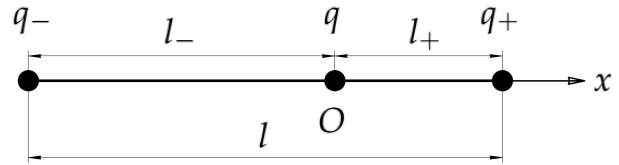


Figure 1: Geometry of problem.

$$l_- = \frac{l_+}{\sqrt{n}}, \quad n = \frac{q_+}{q_-}. \quad (5)$$

If we choose the origin of the  $Ox$ -axis at the equilibrium position of  $q$  and take into account Eq. (5), then its potential energy in the electrostatic field of a system of charges  $q_-$  and  $q_+$  will be as follows:

$$V(\tilde{x}) = k_e \frac{qq_+}{l_+} \frac{f(\tilde{x})}{\sqrt{n}}, \quad (6)$$

where  $k_e$  is Coulomb's constant;  $\tilde{x} = x/l_+$  is the dimensionless coordinate;

$$f(\tilde{x}) = \frac{1}{1 + \sqrt{n}\tilde{x}} + \frac{\sqrt{n}}{1 - \tilde{x}}. \quad (7)$$

Using Eqs. (6), (7) and solving Eq. (2) we get:

$$\tilde{A}_- = \frac{\tilde{A}_+}{1 + (\sqrt{n} - 1)\tilde{A}_+}, \quad (8)$$

where  $\tilde{A}_{\pm} = A_{\pm}/l_+$  ( $\tilde{A}_+ < 1$ ) are the dimensionless amplitudes of the oscillations in this case. In Fig. 2 we plot the dependence  $\tilde{A}_-(\tilde{A}_+)$  for three different values of  $n$ . We see that in all cases for small values of

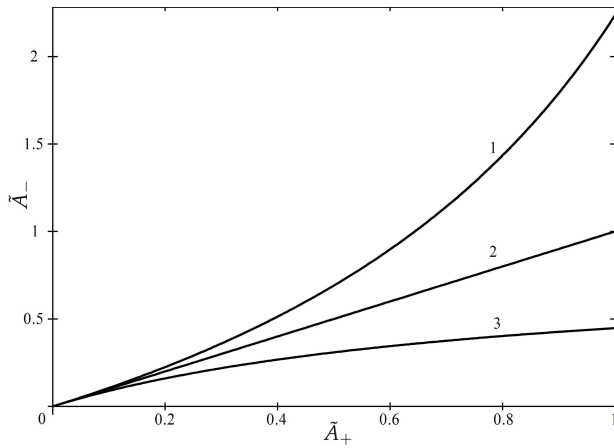


Figure 2: Dependence  $\tilde{A}_-(\tilde{A}_+)$  according to Eq. (8). (1)  $n = 0.2$ ; (2)  $n = 1$ ; (3)  $n = 5$ .

$\tilde{A}_+$  the asymmetry of the oscillations is negligible, i.e.  $\tilde{A}_- \approx \tilde{A}_+$ . If  $\tilde{A}_+$  increases then  $\tilde{A}_-$  becomes smaller than  $\tilde{A}_+$  for  $n > 1$  and vice versa.

Using Eqs. (3), (6) and applying the method for obtaining the period of small oscillations  $T_0$  described in [3] we derive:

$$\frac{T_{\pm}}{T_0} = \frac{\sqrt{n + \sqrt{n}}}{\pi} \int_0^{\tilde{A}_{\pm}} \frac{d\tilde{x}}{\sqrt{f(\pm\tilde{A}_{\pm}) - f(\pm\tilde{x})}} \tag{9}$$

where

$$T_0 = 2\pi \sqrt{\frac{nm l_+^3}{2n(1 + \sqrt{n})k_e q q_+}} \tag{10}$$

(It should be noted that there is the error in work [3]. The numerical coefficient in the right hand side of Eq. (2) and below should be 4 instead of 2). In Fig. 3 we plot dependences  $T_{\pm}(\tilde{A}_+)$  and  $T(\tilde{A}_+)$  calculated numerically using Eqs. (4), (8), (9) for different values of  $n$ . All these functions tend to zero as  $\tilde{A}_+$  approaches to 1. For small values of

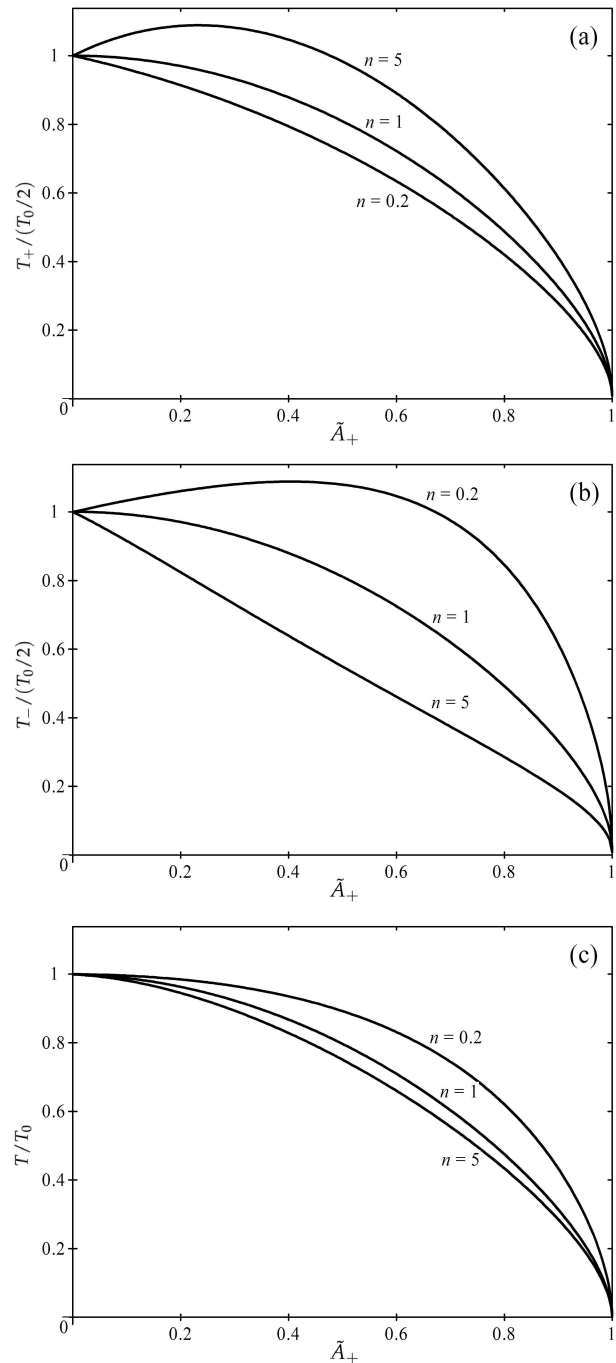


Figure 3: Dependences  $T_+(\tilde{A}_+)$  (a),  $T_-(\tilde{A}_+)$  (b) and  $T(\tilde{A}_+)$  (c), according to Eqs. (4), (8), (9).

$\tilde{A}_+$  function  $T_+(\tilde{A}_+)$  linearly increases (linearly decreases) with the increase of  $\tilde{A}_+$  if

$n > 1$  ( $n < 1$ ). For function  $T_-(\tilde{A}_+)$ , the situation is exactly the opposite. The resulting oscillation period  $T$  (4) does not depend on  $\tilde{A}_+$  for  $\tilde{A}_+ \ll 1$  (see Fig. 3 (c)), that is for the small amplitudes of oscillation the isochronous property takes place.

Using Eq. (6) we can rewrite Eq. (1) in the following form:

$$u_x^2 + \frac{f(\tilde{x})}{\sqrt{n}} = C, \quad (11)$$

where  $u_x = \dot{x}\sqrt{(ml_+)/ (2k_e qq_+)}$  is the dimensionless velocity projection;  $C > f(0)/\sqrt{n}$  is the dimensionless constant. Eq. (11) allows one constructing the phase portrait of oscillations (Fig. 4).

### 3 The Lennard-Jones potential

The Lennard-Jones potential approximates the interaction between a pair of neutral atoms or molecules and has the following form [4]:

$$V(r) = 4\epsilon \left[ \left(\frac{\sigma}{r}\right)^{12} - \left(\frac{\sigma}{r}\right)^6 \right], \quad (12)$$

where  $r$  is the distance between the particles,  $\epsilon > 0$  is the depth of the potential well,  $\sigma$  is the finite distance at which the inter-particle potential is zero. According to Ref. [4] the stable equilibrium position  $r_0 = 2^{1/6}\sigma \approx 1.122\sigma$ .

Let us introduce the dimensionless coordinate  $\rho = (r/\sigma) - \rho_0$ , where  $\rho_0 = 2^{1/6}$ . Then Eq. (11) takes form:

$$V(\rho) = 4\epsilon g(\rho), \quad (13)$$

where

$$g(\rho) = \left(\frac{1}{\rho_0 + \rho}\right)^{12} - \left(\frac{1}{\rho_0 + \rho}\right)^6. \quad (14)$$

It follows from Eqs. (12), (13) that the potential well exists in the interval  $1 - \rho_0 < \rho < \infty$ . Using Eq. (2) we can find numerically  $\tilde{A}_+$  in terms of  $\tilde{A}_-$ , where  $\tilde{A}_\pm = A_\pm/\sigma > 0$  ( $\tilde{A}_- < \rho_0 - 1$ ) are the dimensionless amplitudes of the oscillations in this case. The results of such calculations are presented in Fig. 5. The value of  $\tilde{A}_+$  tends to infinity as  $\tilde{A}_-$  approaches to  $\rho_0 - 1$ . For small values of  $\tilde{A}_-$  the asymmetry of the oscillations is negligible, i.e.  $\tilde{A}_- \approx \tilde{A}_+$ .

Using Eqs. (3), (12) and applying the method for obtaining the period of small oscillations  $T_0$  described in [4] we derive:

$$\frac{T_\pm}{T_0} = \frac{3}{\pi\rho_0} \int_0^{\tilde{A}_\pm} \frac{d\rho}{\sqrt{g(\pm\tilde{A}_\pm) - g(\pm\rho)}}. \quad (15)$$

where

$$T_0 = \frac{\pi\rho_0\sigma}{3} \sqrt{\frac{m}{2\epsilon}}. \quad (16)$$

In Fig. 6 we plot dependences  $T_\pm(\tilde{A}_-)$  and  $T(\tilde{A}_-)$  calculated numerically using Eqs. (14), (15). The values of  $T_+$  and  $T$  tend to infinity as  $\tilde{A}_-$  approaches to  $\rho_0 - 1$ , whereas  $T_-$  remains finite. For small values of  $\tilde{A}_-$  function  $T_+(\tilde{A}_-)$  linearly increases ( $T_-(\tilde{A}_-)$  linearly decreases) with the increase of  $\tilde{A}_-$ . The resulting oscillation period  $T$  (4) does not depend on  $\tilde{A}_-$  for  $\tilde{A}_- \ll \rho_0 - 1$  (see Fig. 6 (c)), that is for the small amplitudes of oscillation the isochronous property takes place.

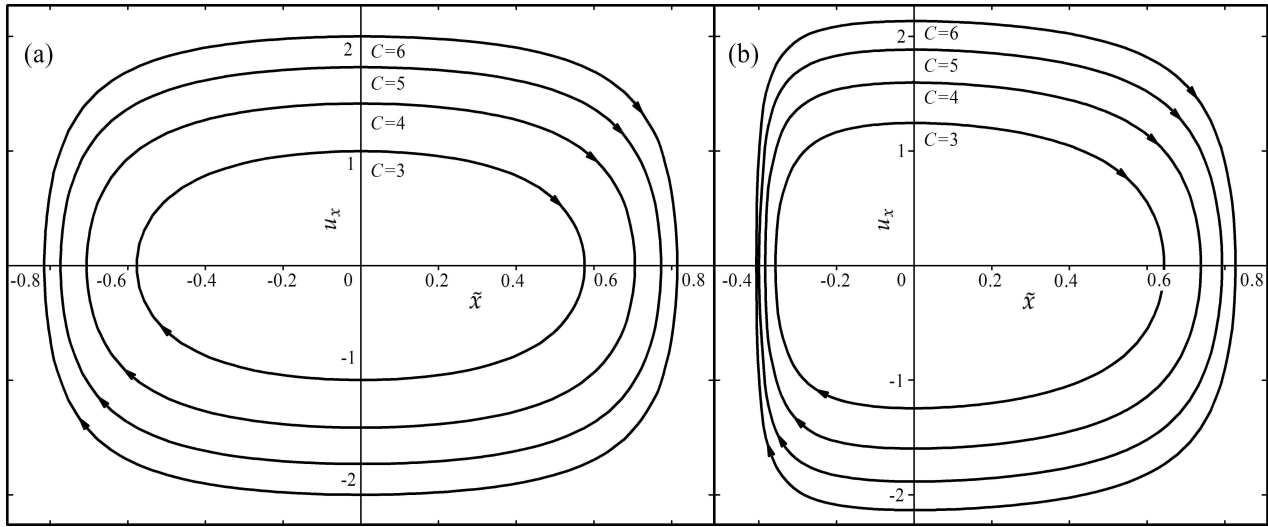


Figure 4: The phase portrait of oscillations according to Eq. (11). (a)  $n = 1$ ; (b)  $n = 5$ .

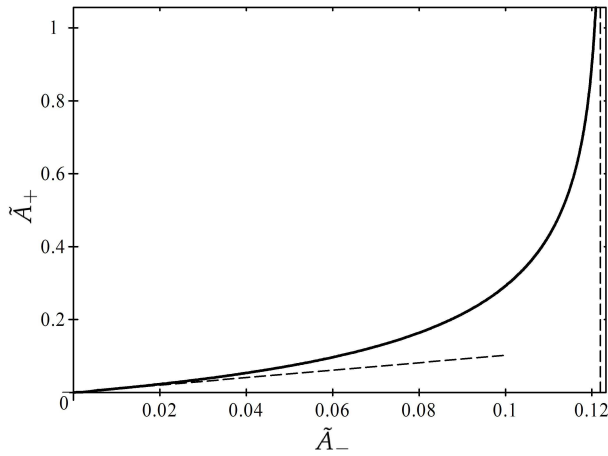


Figure 5: Dependence  $\tilde{A}_+(\tilde{A}_-)$  according to Eqs. (2), (14).

Using Eq. (13) we can rewrite Eq. (1) in the following form:

$$u_\rho^2 + g(\rho) = C, \tag{17}$$

where  $u_\rho = \dot{\rho}\sqrt{m/8\epsilon}$  is the dimensionless velocity projection;  $C > g(0)$  is the dimensionless constant. Eq. (17) allows one constructing the phase portrait of oscillations (Fig. 7). Due to the finite depth of the po-

tential well (13) there is the separatrix  $C = 0$  that separates the phase plane into two distinct areas containing finite (oscillating) and infinite phase trajectories of the particle. The interesting property of this curve is that it approaches asymptotically to  $\rho$  axis as  $u_\rho$  tends to zero.

### 4 Conclusions

In this article we consider usefulness of the law of energy conservation in describing the non-linear oscillations. We show how to apply this fundamental law for finding and constructing amplitude, period, and phase portrait in the case of asymmetric non-linear oscillations. Next, we describe two illustrative examples from electrostatics and molecular physics. These findings will be useful to the students, who study the oscillation phenomena.

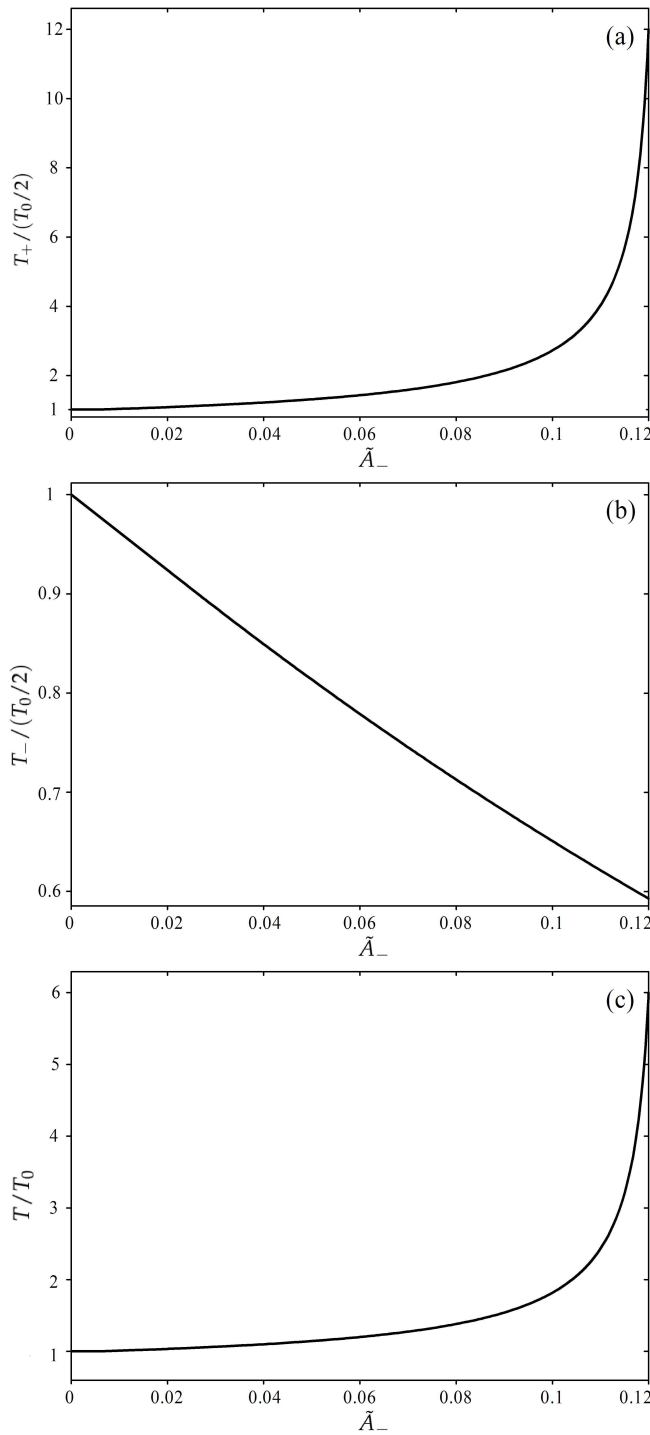


Figure 6: Dependences  $T_+(\tilde{A}_+)$  (a),  $T_-(\tilde{A}_+)$  (b) and  $T(\tilde{A}_+)$  (c), according to Eqs. (4), (14), (15).

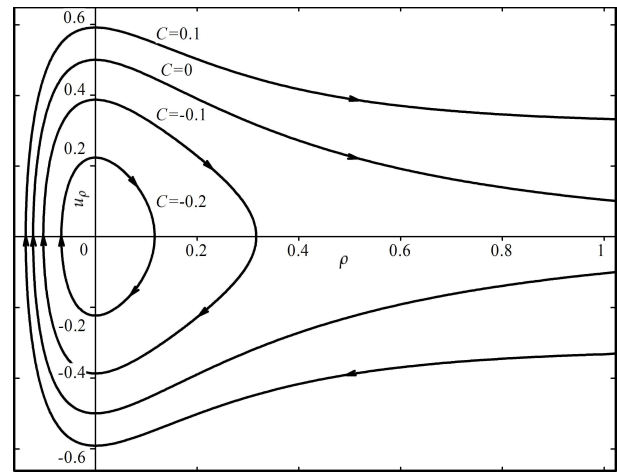


Figure 7: The phase portrait of oscillations according to Eq. (17).

### References

- [1] J. M. Christian (2017). Eur. J. Phys. 38(5), 055002
- [2] Ali H. Nayfeh, Dean T. Mook Nonlinear Oscillations (John Wiley Sons, Inc., 1995)
- [3] Michael A. Waxman (2016). Physics Education 32(1), Article Number: 5
- [4] Ahmed Sayeed (2012). Physics Education 28(4), Article Number: 6

---

# Generalized Lissajous Figures

Rakesh Kumar Pandey

Department of Physics  
Kirori Mal College, University of Delhi  
Delhi - 110007, India.  
rkpandey@kmc.du.ac.in

*Submitted on 22-05-2018*

## Abstract

A simple extension in the graphical technique of drawing Lissajous Figures is proposed in this paper. It is shown how by making a simple modification in the way Lissajous figures are drawn, one can address the requirement of adding two Simple Harmonic Motions which are inclined at an arbitrary angle and are not necessarily perpendicular to each other. It is further added that such a discussion will not only generalize the understanding of superposition of SHMs within the undergraduate classroom teaching but also help the students in developing a clear understanding about the distinction between the 'phase difference' and 'angle of inclination' between two SHMs that is often encountered in the undergraduate students. As an invaluable extension, a condition is also derived in this paper to get a circular motion even when the two SHMs are not perpendicular.

start with, generally, students have a confusion between - the phase difference between the two SHM and - that of the angle of inclination between the two motions. The confusion gets unattended as this superposition is generally discussed under the two specific conditions in most of the standard texts [6],[7],[8] viz. when the two motions are collinear and when they are perpendicular to each other. I prefer emphasizing the point again and again in the undergraduate classroom by saying it in clear words that "the phase difference between the two motions is completely unrelated to the angle between the directions of the two SHMs.

Technically, any SHM can be considered as a superposition of two mutually orthogonal SHMs having no phase difference. In fact, using this understanding one can analyze superposition of any two SHMs that are inclined at an arbitrary angle between them. It would be done in three steps. Firstly, components of one of the two SHMs will be taken parallel and perpendicular to the other SHM. Secondly, the component parallel to the other SHM will be added first to get a resultant SHM in the same direction. Thirdly, the resultant SHM will be added to the other component of the first SHM.

---

## 1. Introduction

Study of superposition of two Simple Harmonic Motions (SHM) [1],[2],[3] finds a very wide application in physics. It is widely used at many places spreading over several topics in physics. The concept is so important [4],[5] that a poor understanding of the phenomenon would hinder in developing a proper clarity of many explanations offered while studying physics. To

As discussed above, in standard undergraduate texts, addition of two SHMs is discussed under the following two conditions.

1. When the two SHMs are collinear and are represented as follows

$$x_1 = A \sin(\omega_1 t + \phi)$$

$$x_2 = B \sin(\omega_2 t + \phi + \delta)$$

Here both the motions are along the x-axis. The resultant of these motions is shown to be always along the same direction and generally another SHM. Normally, the conditions under which the superposition is discussed in standard texts are when  $\omega_1 = \omega_2$  and when  $|\delta|$  is equal to 0, 45, 90 and 180. Simple mathematical analysis is given in all standard texts to give the resultant motion in all possible cases.

2. When the two SHMs are perpendicular to each other and are represented as

$$x = A \sin(\omega_1 t + \phi)$$

$$y = B \sin(\omega_2 t + \phi + \delta)$$

Here the two SHMs are perpendicular as one is along the x-axis but the other is along the y-axis. The conditions, under which this addition is studied, are when  $\omega_1/\omega_2 = n$  (an integer like 1,2,...). In this scenario, the resultant motions are generally two dimensional elliptical motions but under some specific conditions the motion also becomes circular or yet another linear SHM. Again, cases that are normally covered in standard texts are when  $|\delta|$  is equal to 0, 45, 90 and 180. An analytical solution for the resultant motion is extremely complex for general values of  $|\delta|$  and  $n$ . Thankfully, ‘Lissajous Figures’ provides a very effective and very fast graphical technique to solve the problem of adding two perpendicular SHM for any arbitrary value of  $A, B, |\delta|$  and  $n$ .

## 2. Addition of two SHMs inclined at an arbitrary angle

Superposition of two general SHM motions A1 and A2 inclined at an arbitrary angle can be analyzed by making use of the results obtained in the above two cases. In such cases, one can always take components of one of the SHMs such as A1 in the direction of another SHM i.e. A2 and perpendicular to it. The problem will then be solved in two steps. Firstly, the two collinear SHMs A12 and A2 will be added to get a resultant SHM A3 in the same direction. And then, this resultant SHM A3 is added to the other component of the first SHM A11 that is perpendicular to it to get the final resultant.

Superposition of two SHMs in arbitrary directions can be represented by the following two equations.

$$\vec{E}_1 = (A\hat{i}) \sin(\omega_1 t + \phi) \quad (1)$$

$$\vec{E}_2 = (B \cos(\theta)\hat{i} + B \sin(\theta)\hat{j}) \sin(\omega_2 t + \phi + \delta) \quad (2)$$

Here the ‘angle of inclination’ between the two motion is  $\theta$  and the ‘phase difference’ between them is  $\delta$ . Such a representation would provide another chance to reiterate before the undergraduate students that the phase difference  $\delta$  and the angle of inclination  $\theta$  between the two SHMs are completely independent.

To use the analysis done in the two cases as discussed above, one will be advised first to add the following two SHMs in the direction of the x-axis

$$E_{1x} = A \sin(\omega_1 t + \phi) \quad (3)$$

$$E_{2x} = B \cos(\theta) \sin(\omega_2 t + \phi + \delta) \quad (4)$$

to get the resultant  $E_x$  as

$$E_x = A \sin(\omega_1 t + \phi) + B \cos(\theta) \sin(\omega_2 t + \phi + \delta) \quad (5)$$

And then by adding  $E_x$  with

$$E_{2y} = B \sin(\theta) \sin(\omega_2 t + \phi + \delta) \quad (6)$$

one can get the resultant motion. As per the above discussion done above, only in the last step one will be able to use the graphical technique of Lissajous Figures as the two SHMs in this case are perpendicular to each other.

### 3. Generalized Lissajous Figures

In this paper, I propose a generalization of the Lissajous Figures to include addition of two arbitrary SHMs of same frequencies which are not necessarily perpendicular to each other as required normally while using the technique of Lissajous Figure. A simple modification in the idea of drawing Lissajous Figures will help us achieve this generalization.

Generalized self-explanatory diagrams Fig 1, Fig 2, Fig 3 & Fig 4 shown here display addition of two arbitrary SHMs all having a specific angle of inclination ' $\theta$ ' but four different values of  $\delta$  as 0, 45, 90 and 180 degrees. In a single step one can get to the resultant motion wherein one will generally get a tilted elliptical motion.

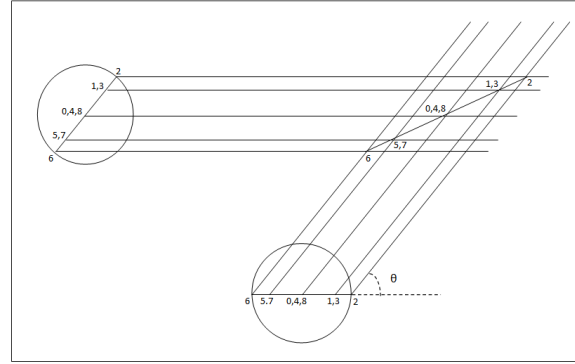


Figure 1: Generalized Lissajous Figure for an arbitrary angle  $\theta$  and  $\delta = 0$  degree. The time period of both the oscillations have been taken as 8 units of time and the positions are marked with numbers 0,1,2,...,8 accordingly in the figure.

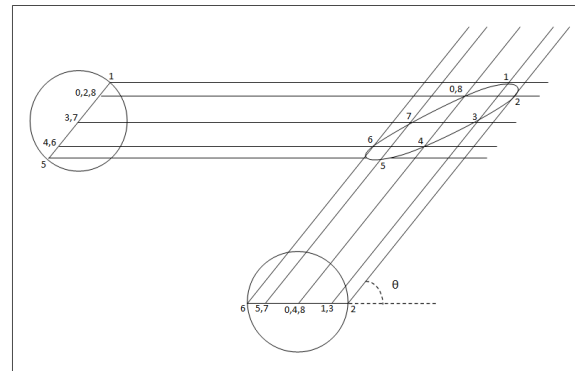


Figure 2: Generalized Lissajous Figure for an arbitrary angle  $\theta$  and  $\delta = 45$  degrees. The time period of both the oscillations have been taken as 8 units of time and the positions are marked with numbers 0,1,2,...,8 accordingly in the figure.

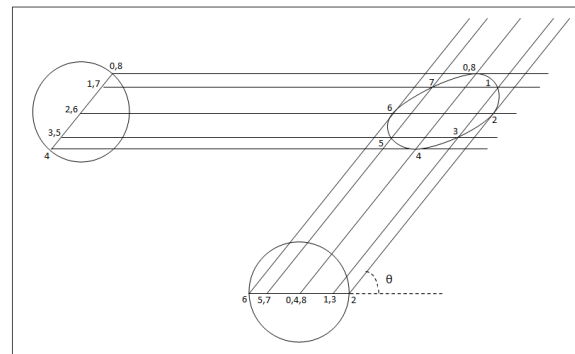


Figure 3: Generalized Lissajous Figure for an arbitrary angle  $\theta$  and  $\delta = 90$  degrees. The time period of both

the oscillations have been taken as 8 units of time and the positions are marked with numbers 0,1,2,....,8 accordingly in the figure.

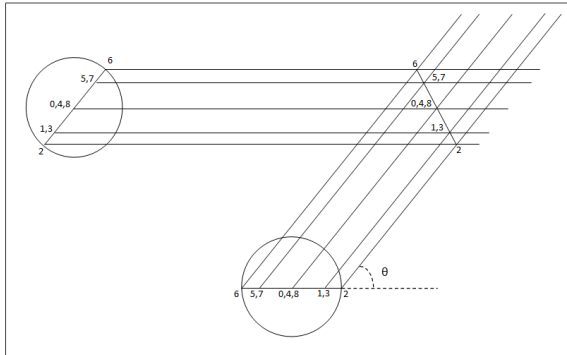


Figure 4: Generalized Lissajous Figure for an arbitrary angle  $\theta$  and  $\delta = 180$  degrees. The time period of both the oscillations have been taken as 8 units of time and the positions are marked with numbers 0,1,2,....,8 accordingly in the figure.

We are aware of the fact that when  $\theta$  is equal to 90 one gets a circular motion when  $\delta$  is also equal to 90 degrees. From the diagrams it appears that for ‘non-orthogonal’ values of  $\theta$  it would be difficult to get a resultant circular motion. It would be interesting to find out the condition under which one would get circular motion even when  $\theta$  is not an integral multiple of  $\frac{\pi}{2}$ .

To find the condition to get a resultant circular motion let us start with two simplifications in the generalized problem that is defined with equations 1 and 2. We take  $\omega_1 = \omega_2 = \omega$  and  $B = A$ . With these simplifications  $E_x$  &  $E_{2y}$  would be written as,

$$E_x = A \cos(\theta) \sin(\omega t + \phi) + A \sin(\theta) \sin(\omega t + \phi + \delta)$$

$$E_x = (A + A \cos(\theta) \cos(\delta)) \sin(\omega t + \phi) + A \cos(\theta) \sin(\delta) \sin(\omega t + \phi)$$

$$E_x = C \sin(\omega t + \phi + \alpha)$$

(7)

where

$$(A + A \cos(\theta) \cos(\delta)) = C \cos(\alpha) \tag{8a}$$

$$A \cos(\theta) \sin(\delta) = C \sin(\alpha) \tag{8b}$$

Also

$$E_{2y} = A \sin(\theta) \sin(\omega t + \phi + \delta)$$

$$E_{2y} = A \sin(\theta) \cos(\delta) \sin(\omega t + \phi) + A \sin(\theta) \sin(\delta) \cos(\omega t + \phi)$$

$$E_{2y} = D \sin(\omega t + \phi + \beta) \tag{9}$$

where

$$A \sin(\theta) \cos(\delta) = D \cos(\beta) \tag{10a}$$

$$A \sin(\theta) \sin(\delta) = D \sin(\beta) \tag{10b}$$

The resultant will be circular motion if  $E_x^2 + E_{2y}^2$  is independent of time. But from eq (7) and (9)

$$E_x^2 + E_{2y}^2 = C^2 \sin^2(\omega t + \phi + \alpha) + D^2 \sin^2(\omega t + \phi + \beta) \tag{11}$$

However from eq. (10a) and (10b) we get,

$$D^2 = A^2 \sin^2(\theta) \tag{12}$$

and

$$\tan(\delta) = \tan(\beta) \tag{17}$$

i.e.

$$\delta = \beta \tag{13}$$

Eq. (8a) and (8b) give,

$$C^2 = A^2 + A^2 \cos^2(\theta) \cos^2(\delta) + 2A^2 \cos(\theta) \cos(\delta) + A^2 \cos^2(\theta) \sin^2(\delta)$$

$$C^2 = A^2 + A^2 \cos^2(\theta) + 2A^2 \cos(\theta) \cos(\delta)$$

Now if

$$\cos(\delta) = -\cos(\theta)$$

i.e. if,

$$\delta = \pi - \theta \tag{14}$$

then

$$C^2 = D^2 = A^2 \sin^2(\theta) \tag{15}$$

Further  $\delta = \pi - \theta$  also simplifies eq. (8a) and (8b) and gives,

$$\cos(\theta) \sin(\delta) / (1 + \cos(\theta) \cos(\delta)) = \tan(\alpha)$$

$$\cot(\theta) = \tan(\alpha)$$

i.e.

$$\alpha = \left(\frac{\pi}{2}\right) - \theta \tag{16}$$

Using Eq. (13), (15) & (16) in Eq. (11) gives,

$$E_x^2 + E_{2y}^2 = A^2 \sin^2(\theta)$$

Which is independent of time and hence represents a circular motion of radius  $A \sin(\theta)$ .

#### 4. Generalised Circular Motion

The derivation given in the above section clearly establishes that when  $\theta = \frac{\pi}{2}$  (The case of traditional Lissajous Figures) then to get a circular motion we must have  $\delta = \frac{\pi}{2}$  (from Eq. (14)) with its radius as the amplitudes of either of the two SHMs.

However, the derivation also predicts that if the two SHMs with equal amplitudes are inclined at an arbitrary angle  $\theta$  degrees, then to get a circular motion the phase difference between the two SHMs of equal amplitudes must be equal to  $\pi - \theta$  degrees. A program was written on SCILAB and was run for angles 20, 50 and 70 degrees and the results confirmed the same.

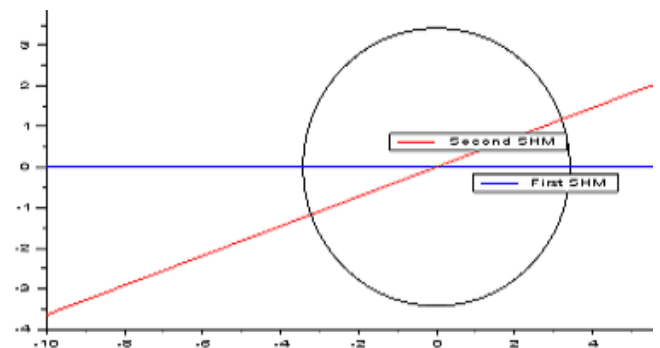


Figure 5: Generalized Lissajous Figure for an angle  $\theta = 20$  degrees and  $\delta = 180 - 20 = 160$  degrees . The resultant is shown to be a circular motion.

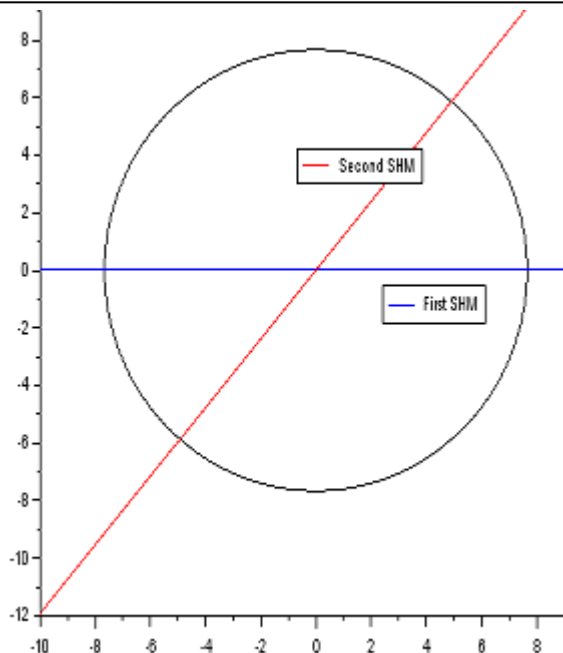
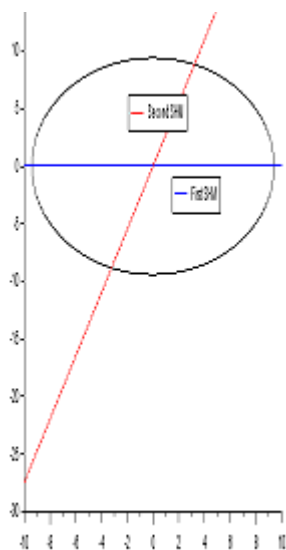


Figure 6: Generalized Lissajous Figure for an angle  $\theta = 50$  degrees and  $\delta = 180 - 50 = 130$  degrees . The resultant is shown to be a circular motion.



The program (SCINOTE):

```
clear
clf
z=input("value for angle (in degrees) between the two SHMs: ");
y=%pi*z/180
a=10
```

```
x=-a:.01:a
plot2d(a*sin(x)*sin(y),a*sin(x+%pi-y)+a*sin(x)*cos(y),style=1);
x=-a:.01:a
plot2d(x,x*sin(%pi),style=2);
x=-a:.01:a
plot2d(x,x*tan(y),style=5);
legends(["First SHM"],[2])
legends(["Second SHM"],[5])
title("Program to add two SHMs inclined at an angle - A- differing in phase by -180-A")
```

In fact except for the case when  $\theta = 0$  all other cases can be analyzed using the Generalized Lissajous Figures and by drawing the diagram for a very small value of  $\theta$  one can actually estimate the case for  $\theta = 0$  quite confidently.

### Acknowledgements

I thank Kirori Mal College to have provided me the environment and facility to carry out this work and compile the same for publication.

### References :

[1] Lissajous figure, Written by: The Editors of Encyclopaedia Britannica,  
<https://www.britannica.com/topic/Lissajous-figure>

[2] Wolfram Mathworld, the web’s most extensive mathematics resource  
<http://mathworld.wolfram.com/LissajousCurve.html>

[3] Lissajous Patterns of CRO or Cathode Ray Oscilloscope  
<https://www.electrical4u.com/lissajous-patterns-of-cro/>

---

[4] Hisham A. H. Al-Khazali, Mohamad R. Askari, Geometrical and Graphical Representations Analysis of Lissajous Figures in Rotor Dynamic System, IOSR Journal of Engineering May 2012, Vol. 2(5) pp: 971-978.

[5] Aaron J. Danner, H. L. Dao, Tom'asTyc, The Lissajous lens: a three-dimensional absolute optical instrument without spherical symmetry, OSA Publishing, Optics Express, Vol. 23, [Issue 5](#), pp. 5716-5722 (2015)

Figure 7: Generalized Lissajous Figure for an angle  $\theta = 70$  degrees and  $\delta = 180 - 70 = 110$  degrees . The resultant is shown to be a circular motion.

<https://doi.org/10.1364/OE.23.005716>

[6] A. P. French, Vibration and Waves, the MIT introductory Physics Series, Chapter 2, page 19-40.

[7] N. K. Bajaj, The Physics of Waves and Oscillations, Tata McGraw Hill, Chapter 2.

[8] Franks S. Crawford, Waves: Berkeley Physics Course, Volume 3, Tata McGraw Hill